



Seafloor Structures and Static Stress Changes Associated With Two Recent Earthquakes in Offshore Southern Batangas, Philippines

Keanu Jershon S. Sarmiento^{1,2*}, Mario A. Aurelio², Paul Caesar M. Flores¹, Anne Drew V. Carrillo¹, Bryan J. Marfito³, Maria Isabel T. Abigania³, Arturo S. Daag³ and Fernando P. Siringan¹

¹The Marine Science Institute, University of the Philippines, Quezon City, Philippines, ²National Institute of Geological Sciences, University of the Philippines, Quezon City, Philippines, ³Department of Science and Technology - Philippine Institute of Volcanology and Seismology (DOST - PHIVOLCS), Quezon City, Philippines

OPEN ACCESS

Edited by:

Gang Rao,
Southwest Petroleum University,
China

Reviewed by:

Yujiang Li,
Ministry of Emergency Management,
China
Wanpeng Feng,
Sun Yat-sen University, China

*Correspondence:

Keanu Jershon S. Sarmiento
kssarmiento@up.edu.ph

Specialty section:

This article was submitted to
Structural Geology and Tectonics,
a section of the journal
Frontiers in Earth Science

Received: 25 October 2021

Accepted: 23 December 2021

Published: 02 February 2022

Citation:

Sarmiento KJS, Aurelio MA, Flores PCM, Carrillo ADV, Marfito BJ, Abigania MIT, Daag AS and Siringan FP (2022) Seafloor Structures and Static Stress Changes Associated With Two Recent Earthquakes in Offshore Southern Batangas, Philippines. *Front. Earth Sci.* 9:801670. doi: 10.3389/feart.2021.801670

The 1994 Mw 7.1 Mindoro Earthquake and the 2017 Mw 5.9 Batangas Earthquake Sequence both occurred in offshore southern Batangas and devastated southern Luzon and Mindoro. These earthquakes exhibited NW-striking right-lateral slip in an area presumably defined by a WNW-striking left-lateral fault, therefore implying the existence of previously unmapped offshore faults. High resolution multibeam bathymetry grid and subbottom profiles revealed a conjugate strike-slip fault system under an approximately EW-directed extension. NW-striking right-lateral faults (F1 Faults: Central Mindoro Fault, Aglubang River Fault, and Batangas Bay Fault System) bound the western part of the study area. On the other hand, a series of almost parallel NE-trending left-lateral and normal faults (F2 Faults: Macolod Corridor, North Verde Fault System, Central Verde Fault System, South Verde Fault, and Northeast Mindoro Fault System) approach the F1 faults from the northeast. The distribution of the 1994 and 2017 earthquakes suggests that the possible rupture areas for these events are the Aglubang River Fault and the southwest Batangas Bay Fault System, respectively. These two traces appear to be connected and a restraining bend is suggested to have acted as a rupture barrier between the two events. Coulomb stress transfer modeling showed that the 1994 earthquake promoted the failure of the 2017 earthquake. Furthermore, results from the stress transfer models showed stress increase on the F1 faults (Batangas Bay Fault System and Central Mindoro Fault) and the northern F2 faults (North Verde Fault System and Central Verde Fault System). The newly recognized faults redefine the knowledge of the neotectonic structure of the area but are still consistent with the ongoing east-west extension in southern Luzon and the overall extension in northern Central Philippines. These faults pose seismic hazards, and more studies are needed to determine their seismogenic potential.

Keywords: submarine faults, conjugate faults, coulomb stress transfer, bathymetry, Philippines

INTRODUCTION

On November 11, 1994, 19:15 GMT, an Mw 7.1 earthquake struck south off Verde Island. An onshore ~35 km-long rupture with right-lateral slip was observed along the Aglubang River Fault in northeast Mindoro. It was accompanied by a tsunami with a maximum vertical runup of 8.5 m (PHIVOLCS Quick Response Team, 1994). The focal mechanism solution of the mainshock exhibits an NNW-trending right-lateral fault which agrees with the observed onshore rupture. The mainshock epicenter and the aftershock distribution point to an offshore extension of the Aglubang River Fault (PHIVOLCS Quick Response Team, 1994). Almost 23 years later, on April 8, 2017 at 07:09 GMT, an Mw 5.9 earthquake event occurred in Batangas Bay, just around 30 km to the northwest of the 1994 mainshock. Relocated hypocenters (Chen et al., 2020) show an NW-trending distribution northeast of Maricaban Island, spanning from Calumpan Peninsula to the northwest down to the mouth of Batangas Bay to the southeast. There have been no reports of onshore rupture. Focal mechanism solution correlated to the northwest trend of the relocated events reveals a northwest-trending right-lateral fault (Chen et al., 2020). The fault

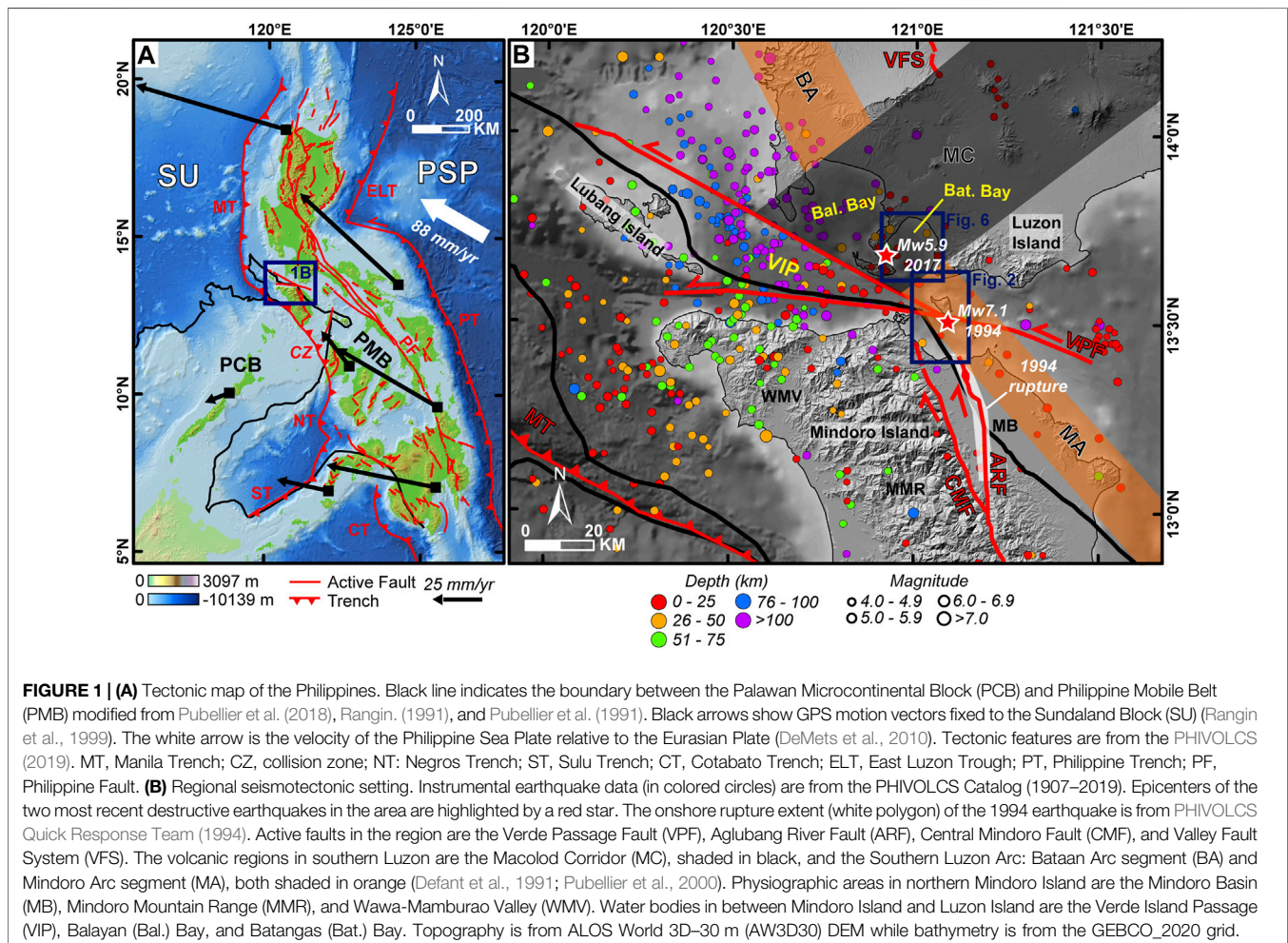
solutions of these destructive earthquakes, however, contrast with what is expected in the area. The only known offshore fault is the WNW-trending Verde Passage Fault which moves in a left-lateral motion.

The proximity of the two earthquake events, the similarity of the focal mechanism solutions, and the disparity from known offshore faults suggest undocumented active structures in offshore southern Batangas. Here we examined the seafloor morphology of Verde Island Passage within the vicinity of Verde Island and of Batangas Bay using a high resolution multibeam bathymetry grid and subbottom profiles to identify potential active faults. We also assessed the coseismic stress transfer of the two earthquake events to the surrounding fault planes using Coulomb Stress Transfer modeling. Finally, the results of this work are used to evaluate the existing ideas on the seismotectonics of the region.

SEISMOTECTONIC SETTING

Regional Setting

The Philippine Mobile Belt is an actively deforming mosaic of terranes sandwiched between the Eurasian Plate/Sundaland



Block to the west and the Philippine Sea Plate to the east (Gervasio, 1967; Aurelio et al., 2013) (**Figure 1A**). The northwestward movement of the Philippine Sea Plate at 88 mm/yr relative to Sundaland Block (DeMets et al., 2010) results in oblique convergence accommodated in a shear partitioning mechanism (Barrier et al., 1991; Aurelio, 2000). Displacement perpendicular to the boundary is accommodated by oppositely dipping subduction zones surrounding the Philippine Mobile Belt. To the west, the east-dipping Manila, Negros, Sulu, and Cotabato Trenches consume the oceanic basins at the margin of the Eurasian Plate while the west-dipping Philippine Trench and East Luzon Trough consume the Philippine Sea Plate in the eastern boundary of the Philippine Mobile Belt. In the central Philippines, the convergence is accommodated by the collision of a portion of Sundaland Block, referred to as the Palawan Microcontinental Block, with the Philippine Mobile Belt (e.g., Pubellier et al., 1997; Yumul et al., 2009; Aurelio et al., 2013). The remaining lateral component of the oblique convergence drives the northwestward translation of the tectonic blocks of the Philippine Mobile Belt mainly facilitated by left-lateral motion along strike-slip faults (Barrier et al., 1991; Aurelio, 2000). Most of the lateral motion is accommodated by the Philippine Fault which spans the entire Philippine archipelago from north to south (Pinet and Stephan, 1990; Ringenbach et al., 1990; Aurelio et al., 1991; Quebral et al., 1996; Tsutsumi and Perez, 2013). However, extensional (Pubellier et al., 1997; Sarewitz and Lewis, 1991; Pubellier et al., 2000) and compressional (Aurelio et al., 2017; Rimando et al., 2019; Rimando et al., 2020) features are also present within the Philippine Mobile Belt, signifying a more complex distribution of shear partitioning (Aurelio 2000; Rimando et al., 2020).

Campaign GPS measurements reveal differential movements of several tectonic blocks within the Philippine Mobile Belt (Rangin et al., 1999; Aurelio, 2000; Yu et al., 2013). In general, displacement vectors from stations east of the Philippine Fault move faster to the northwest compared to those located to the west, with the slowest motions located in the central Philippines (**Figure 1A**). Convergence along the Manila Trench also decreases from north to south as it approaches Mindoro (Rangin et al., 1999; Yu et al., 2013). The slow motion in the central Philippines is attributed to the collision of the Palawan Microcontinental Block to the Philippine Mobile Belt in the Mindoro, Romblon, and Panay area (Rangin et al., 1999; Aurelio, 2000). Overall, these differences in motion can explain several tectonic features in PMB. The slow motion in central Philippines induced shortening, particularly in south-central Philippines. This is evidenced by geologic observations (e.g., young anticlines) and recent thrust/reverse faulting events (Aurelio, 2000; Rimando et al., 2019; Rimando et al., 2020). On the other hand, large differences in motion between the blocks create extension zones, such as in the Macolod Corridor. The extension zones are purported to act as relay zones between the major strike-slip faults that accommodate the northwestward translation (Pubellier et al., 1997; Pubellier et al., 2000).

Local Structures

The study area is in Batangas Bay and Verde Island Passage, in between southern Luzon Island and Mindoro Island (**Figure 1B**). Mindoro consists of accreted continental terranes (belonging to Palawan Microcontinental Block) and the South China Sea ophiolitic crust (Karig, 1983; Rangin et al., 1985; Marchadier and Rangin, 1990; Yumul et al., 2009; Aurelio et al., 2013) while southern Luzon is mainly underlain by Pliocene to Quaternary volcanics belonging to the Philippine Mobile Belt (Defant et al., 1988; Föerster et al., 1990; Mines and Geosciences Bureau, 2010), prompting Karig (1983) to propose an inactive suture in the Verde Island Passage. Focal mechanism solutions and GPS vectors point to a left-lateral movement of a WNW-trending fault within Verde Island Passage. This fault, which is treated as the suture zone based on previous studies (e.g., Karig, 1983), goes by several names (e.g., Verde Passage Suture, Verde Passage Fault, Sibuyan Verde Passage Fault, Lubang Fault), but is referred to here as the Verde Passage Fault. One of the latest traces of the fault from the Philippine Institute of Volcanology and Seismology (PHIVOLCS) starts from the easternmost Verde Island Passage, proceeding west to the south of Verde Island, where it splits into two. One strand continues to the northwest along the coast of southern Batangas while the other one goes in an east-west trend along the coast of northern Mindoro up to Lubang Island. Several works connect the Verde Passage Fault eastward to the Sibuyan Fault, crossing the central Philippines (e.g., Pubellier et al., 1997). Other works also connect Verde Passage Fault westward to the Manila Trench (e.g., Pubellier et al., 2000).

Surrounding onshore structures around Verde Island Passage (**Figure 1B**) are also thought to interact with the Verde Passage Fault. To the north, southern Luzon Island is marked by recent volcanism confined within a NE-trending zone of lineaments and volcanic centers called the Macolod Corridor (Föerster et al., 1990). It spans from the border of Southern Sierra Madre in the northeast and ends in the Maricaban Island in the southwest. The Macolod Corridor has been proposed to connect to the Verde Passage Fault (Pubellier et al., 2000). The southwestern end of the Macolod Corridor also divides the northwest-trending Southern Luzon Arc into the Mindoro Arc segment and the Bataan Arc segment (Defant et al., 1991). Of interest is the Mindoro Arc which consists of volcanic centers spanning from Verde Island up to eastern Mindoro. The age of the Bataan Arc ranges from Pliocene to Recent (Defant et al., 1991) while age dates from the volcanoes in northeast Mindoro range from 0.82 to 1.64 Mya (de Boer et al., 1980). On the other hand, to the south of Verde Island Passage are two active faults situated in onshore northern Mindoro (PHIVOLCS, 2019). The NNW-trending Central Mindoro Fault traverses the center of the island from north to south. The northern half separates the Mindoro Mountain Range from the Mindoro Basin while the southern half traverses through the mountain range. Movement is right-lateral with significant normal component (Mines and Geosciences Bureau, 2010). The Aglubang River Fault branches from the central part of the Central Mindoro Fault toward the northeast in Mindoro Basin which then eventually bends toward the north-northwest as it approaches the northern coast. A right-lateral motion was observed along a ~35 km-rupture during the 1994 Mw 7.1

earthquake. The Aglubang River Fault is proposed to be connected to the Verde Passage Fault (PHIVOLCS Quick Response Team, 1994).

Seismicity

Offshore southern Batangas is prone to earthquakes owing to its proximity to major active tectonic features (**Figure 1B**). In addition to the discussed local structures, the Manila Trench is located more than 100 km to the west and southwest of Verde Island Passage. Most of the earthquakes in the region are thrust-type and come from the subducting slab which extends from the trench to around 80 km beneath Verde Island Passage (Chen et al., 2015). On the other hand, the shallow earthquakes in Verde Island Passage are of the left-lateral strike-slip type which is related to the Verde Passage Fault. Of interest are the 1994 earthquake and the 2017 earthquake sequence. Focal mechanism solutions from these events indicate the existence of NW-trending right-lateral faults which are unknown to the region. Furthermore, these two events exhibit a regional EW extension (Chen et al., 2020), similar to what is observed in the Macolod Corridor to the northeast (Pubellier et al., 2000). Although this active extension is manifested in the structures in the Macolod Corridor, tectonic-related earthquakes are very few within the corridor because of the high geothermal gradient (Pubellier et al., 2000; Chen et al., 2020).

DATA AND METHODS

Interpretation of Seafloor Morphology

For this study, bathymetry data was mainly used to characterize the seafloor morphology of the Verde Island Passage (within the vicinity of Verde Island) and Batangas Bay. An unpublished multibeam bathymetry dataset gridded at 10 m was provided by the National Mapping and Resource Information Authority (NAMRIA). This dataset is a compilation of several hydrographic surveys carried out by the agency. In addition, subbottom profiles were used to complement the interpretations from the bathymetry data. These were acquired using an Edgetech SB-216S, 3100 Portable Subbottom Profiler towed behind M/Y Panata in July 2019. The Edgetech unit operates at 2–15 kHz and achieved decimeter-scale resolution and penetration ranging from a few meters up to 30 m depending on substrate type. Subbottom data was visualized using Hypack 2016 Sub-bottom Processing Feature. Profiles were depth-converted using the standard water velocity of 1500 m/s.

Morphotectonic features were classified into two depending on the level of confidence on its recent activity. A feature is considered a fault when 1) a scarp is prominent, consistent, and continuous along a significant length on a specific trend, 2) there is the presence of offset features and other indicators of motion (e.g., Riedel shears), and/or 3) the feature cuts through sediment or other young morphological features such as submarine terraces. On the other hand, it is considered a lineament when 1) a linear feature is short and displacement cannot be properly discerned, 2) it is modified by erosional processes, and/or 3) the feature is on bedrock. The trends of the mapped structures were analyzed using rose histograms generated via OATools (Kociánová and

Melichar, 2016). In addition to the identified structures in this work, the mapped onshore active faults of PHIVOLCS (2019) in Mindoro Island and the Macolod Corridor structures of Pubellier et al. (2000) were also included in the analysis.

Earthquake Data

Earthquake locations for M 4.0 and above were obtained from the PHIVOLCS Catalog (1907–2019). Relocated earthquakes from the 2017 event were taken from Chen et al. (2020). Aftershock distribution for the 1994 event was digitized from the report of PHIVOLCS Quick Response Team (1994). Focal mechanism solutions were from the Harvard GCMT Catalogue (Dziewonski et al., 1981) with revised locations using the PHIVOLCS Catalog.

Coulomb Stress Transfer Modeling

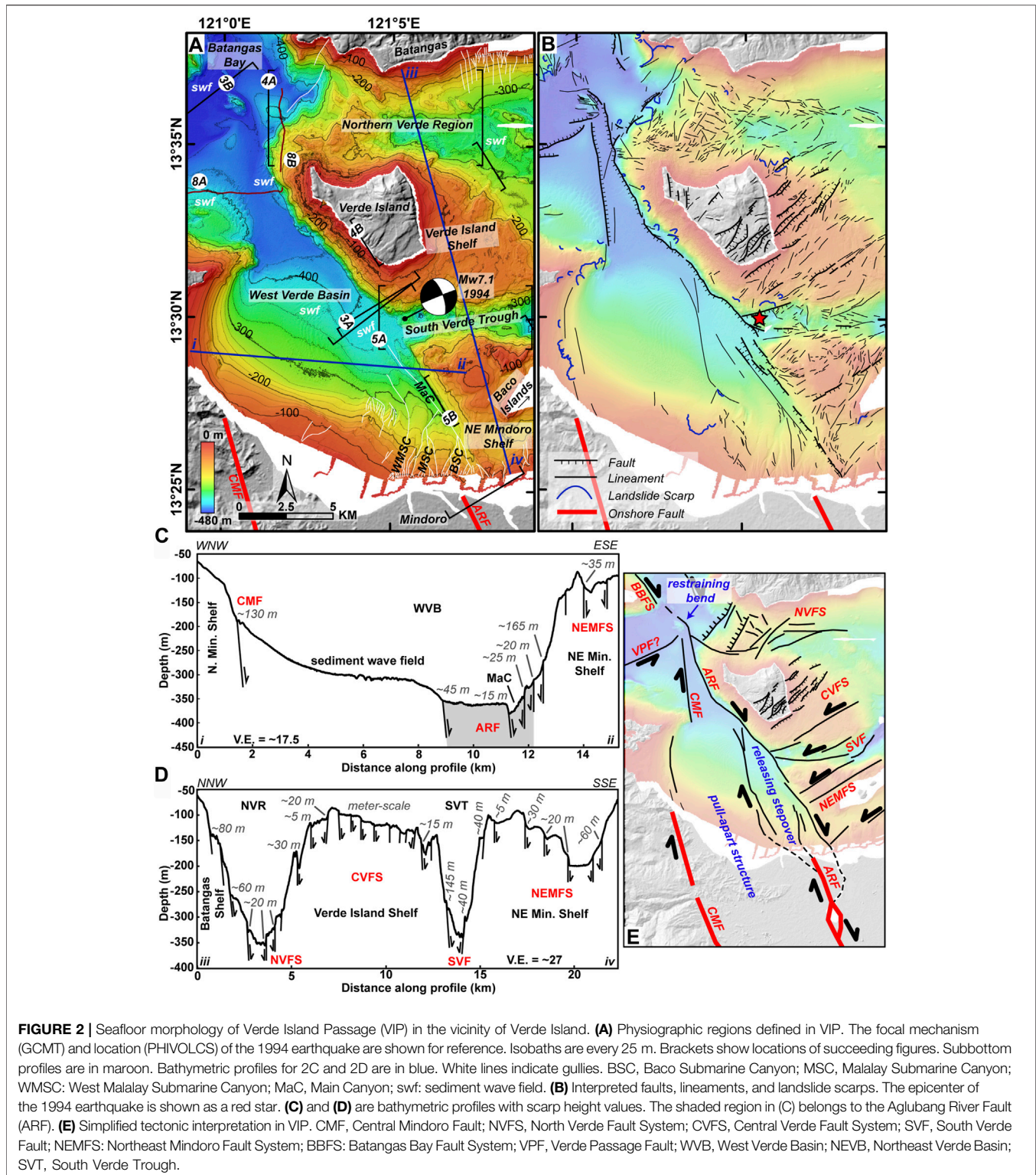
The static stress transfer of the two earthquake events in offshore southern Batangas was analyzed using Coulomb 3.3 (Toda et al., 2011). Coulomb stress change ($\Delta\sigma_f$) is quantified as

$$\Delta\sigma_f = \Delta\tau + \mu'\Delta\sigma_n$$

where $\Delta\tau$ is change in shear stress (positive in the direction of fault slip), $\Delta\sigma_n$ is change in normal stress (positive if the fault is unclamped), and μ' is effective friction coefficient (King et al., 1994; Harris, 1998; Stein, 1999). $\Delta\sigma_f$ is calculated in an elastic half-space (Okada, 1992) assuming Young's modulus of 8×10^5 bar and Poisson ratio of 0.25. μ' is set to 0.4 to minimize uncertainty (King et al., 1994; Toda et al., 1998). A positive $\Delta\sigma_f$ value on a fault plane brings it closer to failure. In contrast, failure is discouraged if $\Delta\sigma_f$ is negative.

With no established rupture models for the 1994 Mw 7.1 event and the 2017 Mw 5.9 event, simple source fault geometry models with uniform slip were constructed using GCMT focal mechanism solutions and fault-scaling relationships (Wells and Coppersmith, 1994). The attitudes of the source faults were based on the NW-trending nodal planes from GCMT. The 1994 Mw 7.1 event has an attitude of $339^\circ/70^\circ/-178^\circ$ (strike/dip/rake) while the fault plane for the 2017 Mw 5.9 event is defined as $314^\circ/85^\circ/176^\circ$ (strike/dip/rake). The source faults were then positioned based on the locations of the interpreted rupture areas, mainshock depth, and aftershock distribution. Other earthquakes between 1994 and 2017 were also considered as source faults. Events were selected by matching the GCMT solutions with the improved locations of the events from the PHIVOLCS Catalog. Source faults were then constructed with the earthquake location as the fault center. The source fault parameters are available in the **Supplementary Material**.

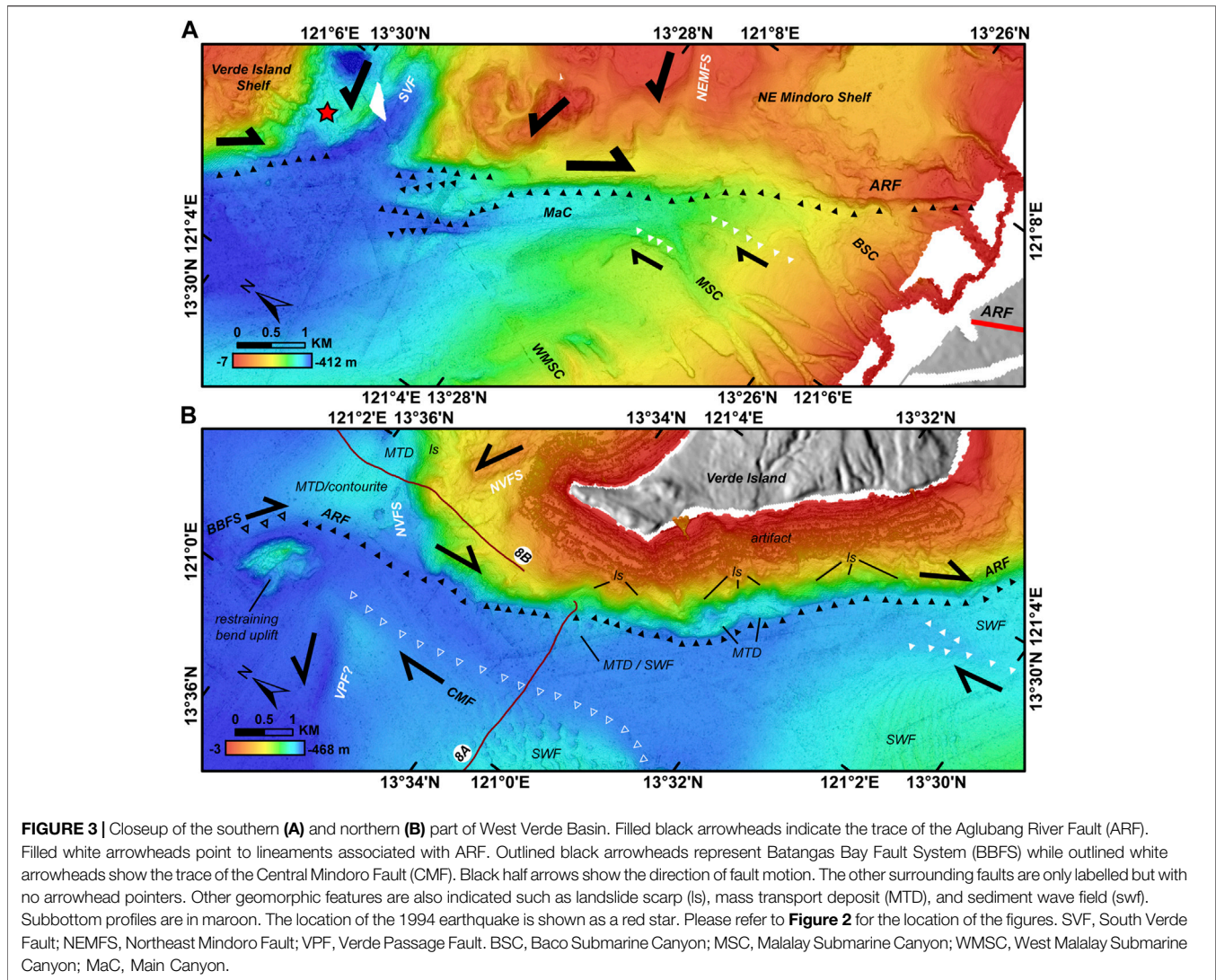
Receiver faults were constructed based on known onshore faults from PHIVOLCS and the prominent offshore faults identified in this work. In the absence of subsurface data, receiver faults were assumed to have simple fault geometry with pure strike-slip or dip-slip motion. The following were the assumed dip/rake for each type of fault: normal = $60^\circ/-90^\circ$, right-lateral = $90^\circ/180^\circ$, and left-lateral = $90^\circ/0^\circ$. The strike, dip, and rake for the source faults derived from the focal mechanism solutions were retained when they acted as receiver faults. Fault widths were assumed to start at 0 km and terminate at 5 km for the short faults and 15 km for the long faults.



Fault planes were subdivided based on length and width to observe the variation of $\Delta\sigma_f$ across the fault plane. The receiver fault parameters are available in the **Supplementary Material**.

Coseismic stress changes of the 1994 earthquake and the 2017 earthquake were calculated on individual receiver faults with

specified rakes to observe the stress imparted by each earthquake to the surrounding fault planes. The distribution of the relocated 2017 earthquakes was also evaluated in terms of static stress changes by correlating it to 1) the cumulative coseismic stress change of the earthquakes from 1994 to pre-2017, and 2) coseismic



stress change from the 2017 earthquake. The receiver fault for both models was set to the fault plane of the 2017 mainshock and calculated at the depth of the mainshock (14.3 km).

Only coseismic stress change is considered in this study. It is acknowledged that other factors, such as postseismic stress change and interseismic loading, also contribute to the stress received by the fault planes. However, these types of analyses require data, such as crustal rheological parameters and long-term geodetic data (e.g., Wang et al., 2006; Li Y et al., 2020), that are absent in the study area, marking a major limitation in the analysis of stress changes.

RESULTS

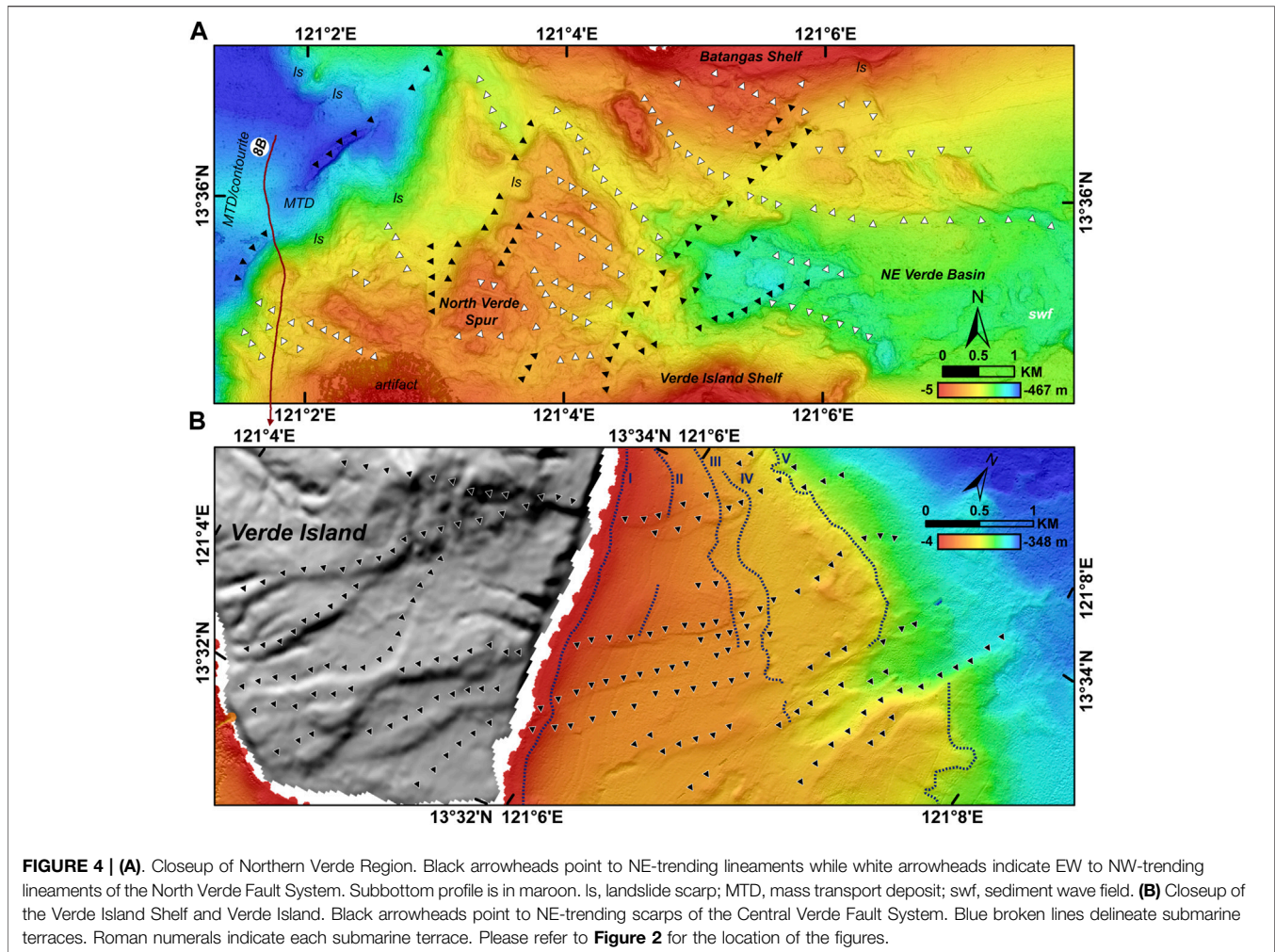
Seafloor Morphology

The seafloor in the Verde Island Passage in the vicinity of Verde Island is divided into five physiographic regions (**Figure 2A**) based on its geomorphology and structures (**Figure 2B**).

Bathymetric profiles across these regions and the interpreted neotectonic structure are also shown in **Figures 2C–E**. The regions and structures are herein referred to as the 1) West Verde Basin with the Aglubang River Fault and Central Mindoro Fault (**Figure 3**); 2) Northern Verde Region with the North Verde Fault System (**Figure 4A**); 3) Verde Island Shelf with the Central Verde Fault System (**Figure 4B**); 4) South Verde Trough with the South Verde Fault (**Figure 5A**); and 5) Northeast Mindoro Shelf with the Northeast Mindoro Fault System (**Figure 5B**). To the northwest, Batangas Bay hosts the Batangas Bay Fault System (**Figure 6** and **Figure 7**). Subbottom profiles supporting the morphological interpretations are shown in **Figure 8**. Below, the seafloor morphology and interpreted faults per region are discussed.

West Verde Basin

The West Verde Basin is an NW-elongated depression situated in between Verde Island and the northernmost point of Mindoro Island (**Figure 2A**). A prominent NW-trending (N40°W to



N10°W) steep linear bathymetric escarpment bordering the NE Mindoro Shelf and the Verde Island Shelf defines the eastern boundary of the West Verde Basin. To the west and to the south, the West Verde Basin is delimited by the arcuate insular slopes of northern Mindoro. To the southeast, the Baco River and the Malaylay River drains to the Baco Submarine Canyon, Malaylay Submarine Canyon, and West Malaylay Submarine Canyon (Sequeiros et al., 2019). The gullies of the three canyons mostly trend from N to NNE. Baco and Malaylay Submarine Canyons merge into the Main Canyon. The latter runs along the base of the NW-trending escarpment and exits to the West Verde Basin (**Figure 3A**). The West Malaylay Submarine Canyon, on the other hand, diverts to the NW before it joins the West Verde Basin. The southern part of the West Verde Basin is ~8 km wide with depths ranging from ~275 m in the south to around ~425 m in the center of the basin. The basin narrows to ~1 km and deepens to ~450 m in its northernmost part. A small bathymetric relief (~100 m-high, ~1 km-wide) punctuates the basin in the northernmost end. Wide swaths of sediment waves (1–4 km) characterize the basin floor. A ~2 km-wide sediment wave field is also found at the western border of the northern West Verde Basin. Meanwhile, the insular slopes bounding the West Verde

Basin are indented with arcuate landslide scarps. Corresponding mass transport deposits were observed at the toe of the landslide scarps in the Verde Island Shelf (**Figure 2B**). Several sediment wave fields are located adjacent to the mass transport deposits or at the toe of the scarp and might indicate remobilization of mass transport deposits by bottom currents.

The right-lateral Aglubang River Fault terminates in Malaylay Island (PHIVOLCS Quick Response Team, 1994), in the vicinity of the Baco River, where it trends at around N25°W. Immediately offshore, the continuation cannot be properly observed because of the active sedimentary processes in the submarine canyons. The resolution of the bathymetry data also prevents accurate observation of scarps related to the 1994 rupture. However, the NW-trending escarpment bounding the West Verde Basin is just located less than 2 km to the northeast of the Aglubang River Fault (**Figures 2B,E; Figure 3A**). It is proposed here that this prominent escarpment is part of the Aglubang River Fault. Although no right-lateral movement was observed, the consistency of the trend and proximity to the mainshock makes it a likely candidate. Moreover, fault-scaling relationships (Wells and Coppersmith, 1994) for the 1994 Mw 7.1 earthquake suggest an additional ~37 km rupture to the

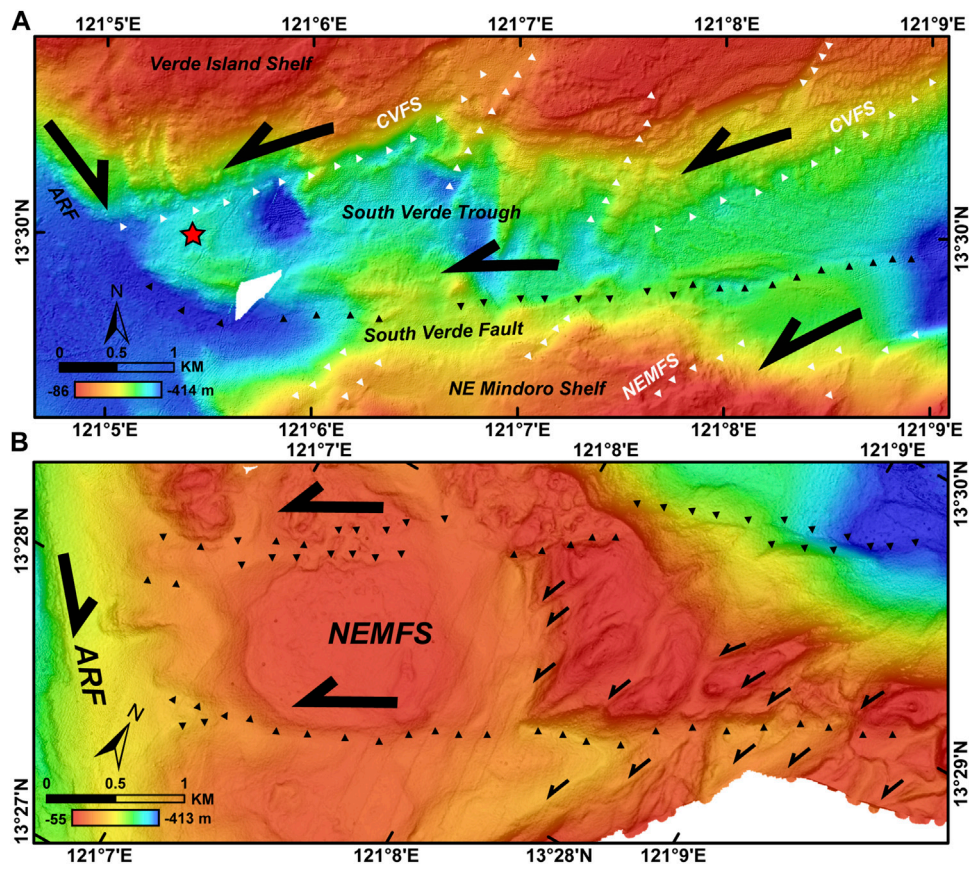


FIGURE 5 | (A) Closeup of the South Verde Trough. Black arrowheads show the trace of the South Verde Fault. White arrowheads point to the NE-trending structures of the Central Verde Fault System (CVFS) and Northeast Mindoro Fault System (NEMFS). Black half arrows indicate fault motion. The epicenter of the 1994 earthquake is shown as a red star. **(B)** Closeup of the Northeast Mindoro Shelf. Black arrowheads point to the longer faults of NEMFS. Smaller half arrows indicate the motion of shorter faults (Riedel shears). Please refer to **Figure 2** for the location of the figures. ARF, Aglubang River Fault.

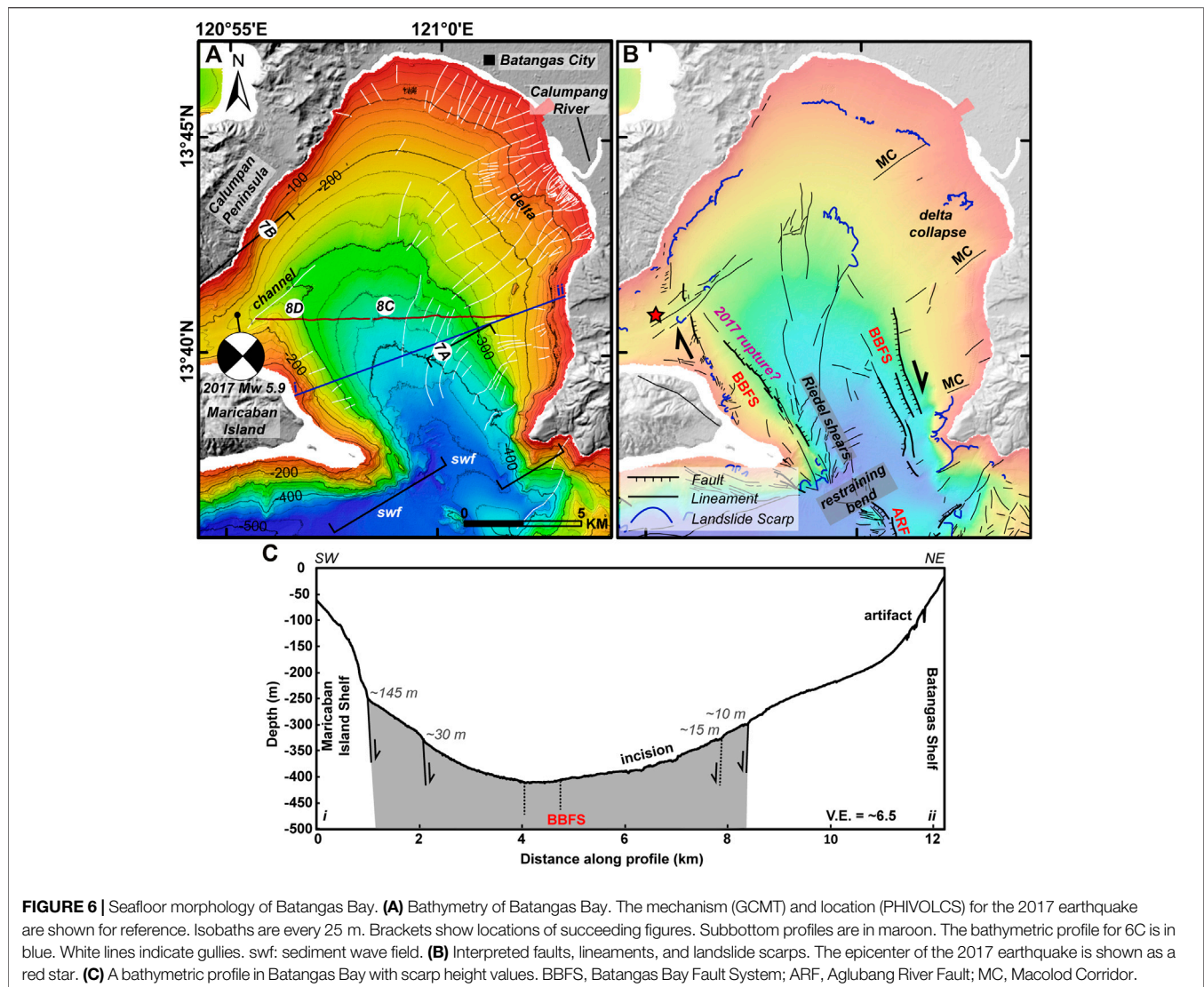
observed 35 km onshore rupture (PHIVOLCS Quick Response Team, 1994). The offshore escarpment reaches to around 25 km in length. A ~12 km-long segment must then exist to complete the estimated additional ~37 km rupture. This segment could be located in the southern onshore Aglubang River Fault, where rupture is proposed to have propagated but was not documented (PHIVOLCS Quick Response Team, 1994).

The right-stepping nature necessitates a releasing stepover zone in between the two right-lateral faults (**Figure 2E**). Lineaments define a depressed zone where the submarine canyons are located. NNW-trending lineaments bound the submarine canyons to the west. These lineaments continue to the West Verde Basin where a ~45 m-high lineament separates the sediment wave field to the west and a deeper part of the West Verde Basin to the west. Lineaments were also observed in the submarine canyon area but are too modified (**Figure 3A**). The trends of the submarine canyons might also be structurally controlled. Overall, the structural pattern points to right-lateral shearing. Onshore, the rivers in the vicinity of the Aglubang River Fault might also have exploited pre-existing structures. If this is the case, the rivers drained toward the pull-apart zone where the submarine canyons developed.

Scarp heights along the offshore Aglubang River Fault vary along its length. Scarps along the border of NE Mindoro Shelf range from 20 to 130 m while the height is mostly around 400 m in the Verde Island Shelf. In between the two shelves is the South Verde Trough where the trace of the Aglubang River Fault at South Verde Trough's western end is modified by erosional processes. Remnant scarps are around 25 m high.

Northwest of Verde Island Shelf, the trace of the Aglubang River Fault bends to a more northerly trend (N10°W) and is manifested by a ~25 m-high scarp. As the Aglubang River Fault approaches the bathymetric relief at the northernmost end of West Verde Basin (**Figure 3B**), the trace bends to the NW (N45°W). The relief at the site of the change in trend probably is an uplift resulting from a restraining bend. This bathymetric relief could also be an old volcanic center. In any case, the change in trend is also reflected in the lineaments dissecting this feature. The Aglubang River Fault is proposed to end before the change in trend. The lineament with a more northwestern trend is proposed to belong to the Batangas Bay Fault System. This will be explained in the later section.

The Central Mindoro Fault also ends at the northern coast of Mindoro (**Figure 2**). Immediately offshore at roughly the same



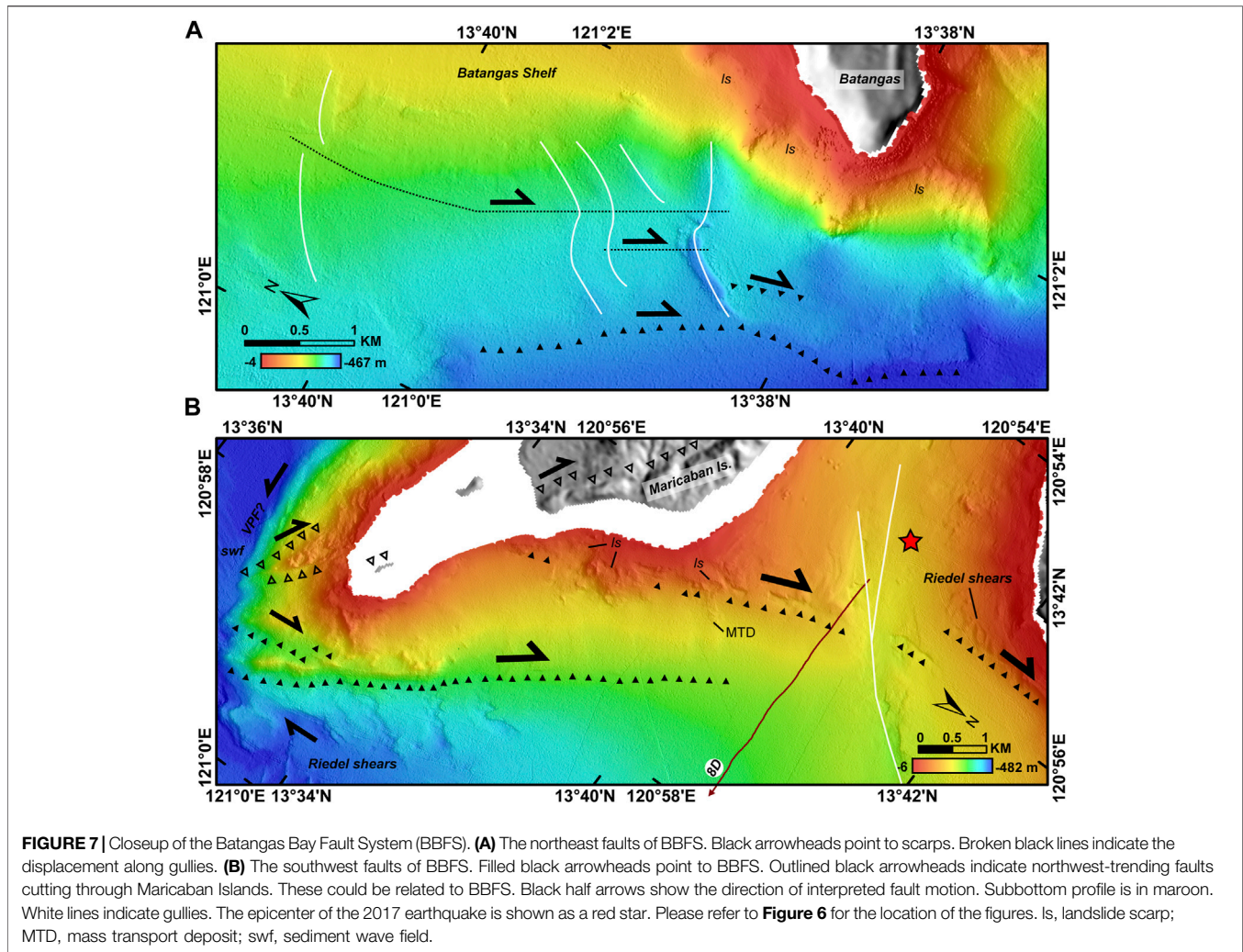
trend is the insular slope separating the Northern Mindoro Shelf and the West Verde Basin. This is consistent with the onshore Central Mindoro Fault which separates the Mindoro Mountain Range from the Mindoro Basin. Further north, a 15–25 m-high lineament bounds West Verde Basin and separates the basin from a sediment wave field to the west (Figure 2, Figure 3B, Figure 8A). This lineament could be part of the Central Mindoro Fault. Further to the west of the sediment wave field, a NE-trending lineament was observed which converges with the Central Mindoro Fault near the bathymetric relief at the northern end of the West Verde Basin. This feature could be related to the Verde Passage Fault or could be a new feature that deserves further investigation in the future.

Overall, both the Aglubang River Fault and Central Mindoro Fault bound the West Verde Basin. Considering that the Aglubang River Fault splits from the Central Mindoro Fault in a right-stepping manner in central Mindoro Island, this creates a pull-apart structure that includes the West Verde Basin and a part of the Mindoro Basin (Figure 2E). A nested pattern of pull-apart

zones is recognized: 1) the West Verde Basin-Mindoro Basin in between the Central Mindoro Fault and Aglubang River Fault; 2) the Aglubang River Fault releasing stepover; and 3) the Baruyan Lake (PHIVOLCS Quick Response Team, 1994) along the Aglubang River Fault.

Northern Verde Region

The Northern Verde Region has a complex morphology primarily composed of a spur and a basin (Figure 2, Figure 4A). The North Verde Spur is 150–280 m deep and ~6 km wide. It has a rough surface littered with mounds and linear ridges. It is attached to the Verde Island Shelf to the south and is separated by a narrow gap (<1 km) from the Batangas Shelf to the north. The western boundary of the spur is a NE-trending lineament which steeply drops to more than 400 m depth near the mouth of Batangas Bay. At the foot of the linear boundary is a moat and mounded drift pair typical of contourite systems (Figure 8B). Landslide scarps (0.1–1 km wide) are present in the spur and are largest in the western boundary (Figure 2B).



Corresponding mass transport deposits are observed downslope and near the contourite drifts, implying reworking of mass transport deposits by bottom currents.

To the east, the North Verde Spur transitions to the Northeast Verde Basin (**Figure 4A**). This basin is delimited by the 300 m isobath and might extend further to the east. The basin floor has numerous circular depressions (100–300 m wide) which are probably products of bottom current processes. A sediment wave field is observed in the eastern part. The northern part of the basin is bounded by a rectangular bathymetric relief (~50 m high) attached to the Batangas Shelf. To the south is the Verde Island Shelf.

Two main lineament trends dissect the Northern Verde Region (**Figure 4A**). The first main trends are at $N40^{\circ}E \pm 10^{\circ}$ while the other trends are at $N60^{\circ}W \pm 30^{\circ}$. The NW lineaments cut through the whole Northern Verde Region while the NE lineaments dissect the spur more heavily than the basin. The lineaments are interpreted to have normal displacements (**Figure 2D**, **Figure 8B**) with a possible strike-slip component. The two main lineament trends might be conjugate structures. All

lineaments are collectively referred to as the North Verde Fault System.

Verde Island Shelf

The Verde Island Shelf has an unequal width around the island (**Figure 2**, **Figure 4B**). The northern shelf is only around 0.5 km wide before it transitions to the Northern Verde Region. The western side is also <1 km wide along the Aglubang River Fault. In contrast, the eastern and southern side reaches up to ~4 and ~6.5 km, respectively. The shelf has a relatively gentle slope (~5°), except around scarps, gullies, and localized mounds. Five submarine terraces were observed in the eastern shelf with the following depths of the terrace outer edge: I = 15–20 m, II = 50–60 m, III = 85–100 m, IV = 110–120 m, and V = 140–170 m.

NE-trending structures ($N50^{\circ}E \pm 10^{\circ}$) dissect the shelf, particularly in the eastern and southern sides. These are collectively called the Central Verde Fault System. Structures cannot be observed in the northern and western shelves because of processing artifacts. On the eastern shelf, the Central Verde Fault System structures are short (<2 km long) and closely spaced

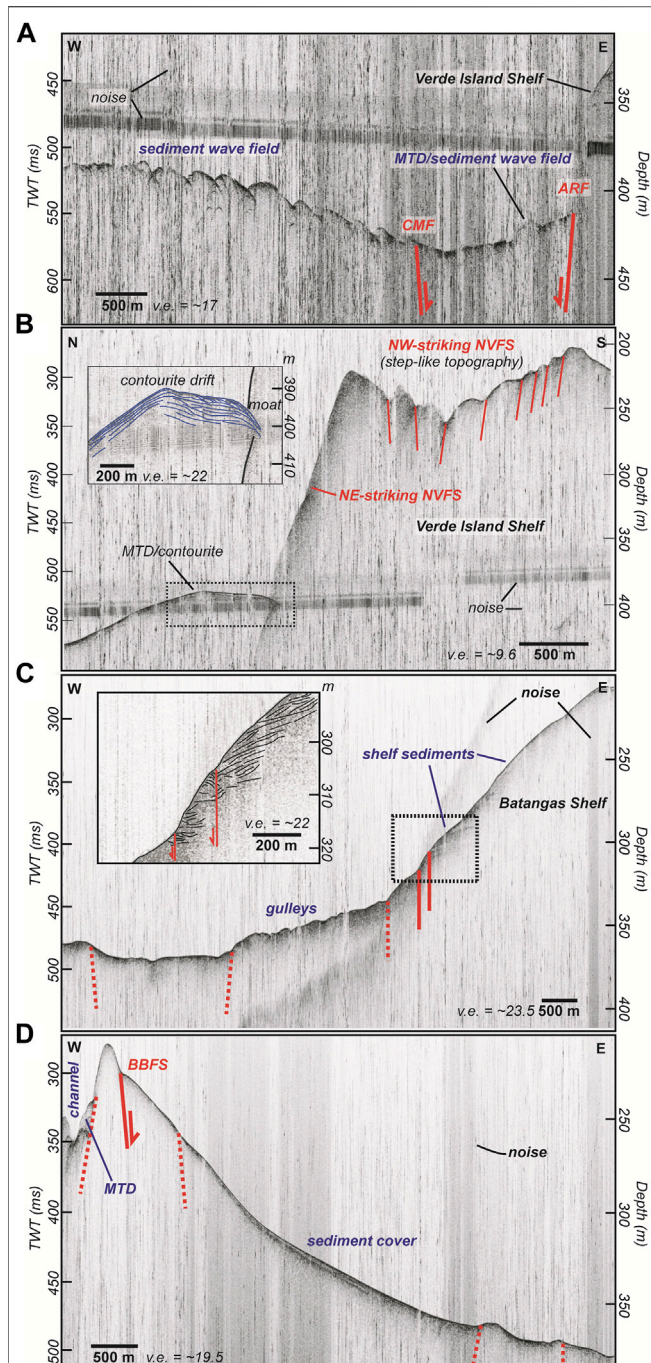


FIGURE 8 | Subbottom profiles in (A) West Verde Basin, (B) Northern Verde Region, and (C,D) Batangas Bay. See text for discussion. Depth was calculated using a velocity of 1500 m/s. Locations of the profiles are in **Figure 2** and **Figure 6**. ARF, Aglubang River Fault; CMF, Central Mindoro Fault; MTD, Mass Transport Deposit; NVFS, North Verde Fault System; BBFS, Batangas Bay Fault System.

(<1 km apart). They show normal displacement ranging from <10 m in the shallower parts to ~40 m at the edge of the shelf. The faults cut through the submarine terraces, implying recent activity. The terraces become more fragmented with depth

which might partly be due to fault activity. Moreover, the structures continue onshore Verde Island where they cut through the volcanic center and apron, with displacements ranging from <10 to 60 m. On the other hand, in the southern shelf, lineaments are shorter and less clear, except for a ~9 km fault which spans from the eastern shelf boundary up to the South Verde Trough. This fault displays left-lateral motion.

South Verde Trough

The South Verde Trough is a ~2 km-wide, EW-elongated depression separating the Verde Island Shelf and NE Mindoro Shelf (**Figure 2**; **Figure 5A**). The trough might continue to the east. Seafloor bathymetry is quite complex. Irregularly shaped depressions with depths up to 400 m are randomly distributed in the seafloor. Promontories from surrounding shelves protrude toward the trough. At the center of the trough is a 40–90 m-high EW-trending ridge. The fault associated with this ridge is referred to as the South Verde Fault. A left-lateral motion is inferred. NE-trending structures from the Verde Island Shelf and NE Mindoro Shelf converge toward the South Verde Fault. The structural pattern suggests that the NE structures are acting as R shears of a left-lateral fault. Other lineaments of varying trends projecting toward the South Verde Fault might be antithetic shears. South Verde Fault bends to a more NW trend as it approaches the Aglubang River Fault.

NE Mindoro Shelf

The NE Mindoro Shelf is a wide shelf that spans the entire area of northeast Mindoro and appears to be connected to the Mindoro Basin (**Figure 2**; **Figure 5B**). The Baco Islands, three small islands arranged in a northeast trend, are located at the center of the shelf. The study site is located between the Aglubang River Fault and the Baco Islands. Depth reaches up to 275 m. Plateaus (~100 m depth) and mounds (~50 m depth) dominate the northwest area. To the south, gullies drain from the coast toward a small NE-trending basin. This basin is delimited by the 175 m isobath and is only around 1–2 km wide. Depressions and sediment waves characterize the seafloor.

NE-trending structures dissect the whole shelf. The longer faults trend $N55^{\circ}E \pm 5^{\circ}$ and delineate the borders of the plateaus and the small basin. On the other hand, the shorter lineaments mainly trend $N30^{\circ}E \pm 10^{\circ}$ and approach toward the longer lineaments. The morphology suggests left-lateral motion with the shorter structures acting as R shears. Collectively, these structures are referred to as the NE Mindoro Fault System. This fault system continues to the South Verde Trough to the NE. To the SW, the NE Mindoro Fault System approaches Aglubang River Fault, where several of these structures bend to the NW.

Batangas Bay

Batangas Bay is a ~14 km-wide and ~18 km-long water body indented in southern Luzon Island (**Figure 6A**). It is bounded by land on its western, northern, and eastern sides. Maricaban Island is located on its southwestern side. A narrow waterway (~3 km) in between Maricaban Island and Calumpan Peninsula connects Batangas Bay to Balayan Bay. A ~7.5 km-wide mouth is located at the southern part of the bay, leading to Verde Island Passage.

The bay is around 100 m deep at the shelf edge and gently deepens ($\sim 5^\circ$ slope) up to around 450 m at the mouth of the bay. The shelves surrounding the bay are very narrow. It ranges from 0.1 to 1 km on the western, eastern, and southeastern sides. The northern side, on the other hand, is 1–3 km wide. A 4 km-wide delta of the Calumpang River is also present on the northeastern shelf. Subbottom profiles across the bay show sediment cover generally thinning toward the bay center where there are abundant gullies (**Figures 8C,D**). Small, closely spaced landslide scarps (<300 m wide), with occasional corresponding mass transport deposits, indent the northern, western, and southwestern shelves (**Figure 6B**, **Figure 7**, **Figure 8D**). A delta collapse feature (~ 500 m wide) is also present in the northeastern shelf (**Figure 6B**). Larger landslide scarps (300–800 m) are observed on the southeastern shelf. Gullies heavily incise the bay, particularly at the vicinity of the delta. To the west, a northeast-trending channel (~ 500 m-wide) connects to the passage to Balayan Bay. Sediment wave fields are present within the channel, at the toe of the delta collapse, and at the mouth of the bay.

Batangas Bay is mainly cut by faults trending $N30^\circ W \pm 15^\circ$ (**Figure 6B**). These faults are collectively called the Batangas Bay Fault System. The fault system is only located in the southern half of the bay. Parallel faults and lineaments (~ 0.75 –5 km long) cut through the southeastern insular slope and displace the gullies horizontally (~ 20 –100 m) (**Figure 7A**). Scarp heights range from 1 to 15 m. A subbottom profile crossing the southeastern shelf (**Figure 8C**) revealed shelf sediments displaced in a normal motion (<1 m). Two main faults straddle the southwestern part of the bay, along Maricaban Island (**Figure 7B**). One fault ($\sim N40^\circ W$) starts as a linear ridge (~ 50 m high, ~ 3 km long) at the mouth of the bay and then continues as smaller scarps (~ 5 –20 m high, ~ 6 km long total) along the base of the insular slope. The other fault defines the shelf edge for about 5 km. The trace is obscured by numerous slope failures across its length. A subbottom profile across the Maricaban slope (**Figure 8B**) did not image the fault because of thin sediment cover. Two traces (~ 1 km long) continue toward the Calumpang peninsula shelf. No onshore trace continuation was observed. The 2017 earthquake sequence plots near southwest Batangas Bay Fault System, implying that at least one of the traces corresponds to the fault rupture.

In the bay center, numerous lineaments are in between the main SW and NE fault strands (**Figure 6B**). Some of the lineaments correspond to the gullies. Parallel lineaments approach the SW faults, with the pattern suggesting these are Riedel shears of a right-lateral fault. It is therefore inferred that the lineaments in the bay center accommodate the shearing of Batangas Bay Fault System. Moreover, several structures ($N75^\circ W \pm 5^\circ$) branch from the eastern edge of the Maricaban shelf toward the Maricaban island. These structures, along with SW Batangas Bay Fault System, appear to project toward the bathymetric relief at northern West Verde Basin. This implies that Batangas Bay Fault System connects to the bathymetric relief and Aglubang River Fault. The connection in between, however, is covered with sediment waves.

Several NE-trending lineaments ($\sim N55^\circ E$) are also present particularly in the northeastern part of the bay near the delta

(**Figure 6**). The gullies in the delta and the channel southwest of the bay also trend to the northeast. Traditionally, Batangas Bay is considered part of the Macolod Corridor and the NE structures might be related to this tectonic zone.

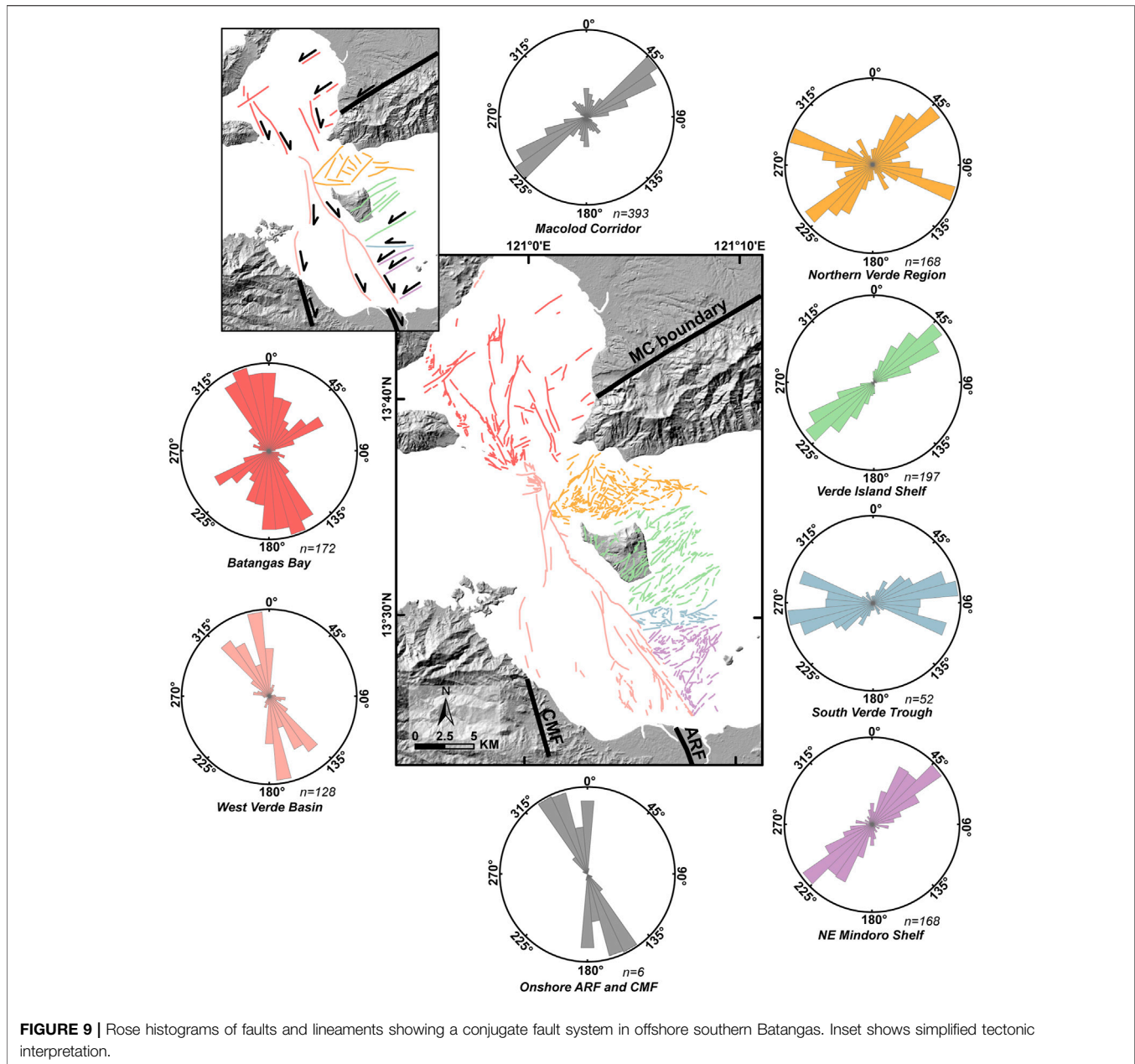
Summary

Seven fault systems were defined in offshore southern Batangas with clear contrast in trend and motion (**Figure 9**). The overall pattern of the mostly left-lateral NE-trending fault systems (F2 faults), including the Macolod Corridor, and the right-lateral NW-trending fault systems (F1 faults) suggest a conjugate fault system in a WNW-ESE to EW-directed extension. Earthquakes from the PHIVOLCS Catalog (>Ms 4.0) show that most of the earthquakes in the region of interest are concentrated in the Aglubang River Fault and the southwest Batangas Bay Fault System, mostly corresponding to the 1994 earthquake and 2017 earthquake sequence, respectively (**Figure 10A**). A 1997 Mw 5.4 earthquake occurred near the restraining bend of the F1 faults (**Figure 10A**). Very few earthquakes are plotted in the other defined structures. The 1994 and 2017 events appear to be delimited by the interpreted restraining bend of the Aglubang River Fault and the Batangas Bay Fault System (**Figure 10B**).

Static Stress Transfer

Coulomb stress transfer modeling for the 1994 Mw 7.1 rupture along the Aglubang River Fault showed stress increase in the northern and southern region of the source fault (**Figure 11A**). The fault plane along the 2017 Batangas Bay Fault System rupture area was brought >0.5 bars closer to failure. Other faults in the northern region with positive stress change are: Batangas Bay Fault System (~ 6 bars), normal North Verde Fault System (>4.2 bars), and normal Central Verde Fault System (>0.8 bar). In the southern part, a small portion of the Central Mindoro Fault had a stress increase at >1.8 bars. The other receiver faults along the sides of the Aglubang River Fault showed stress decrease ranging from -0.02 to -12.9 bars. In general, stress change is largest near the ends of the source fault and decreases with distance.

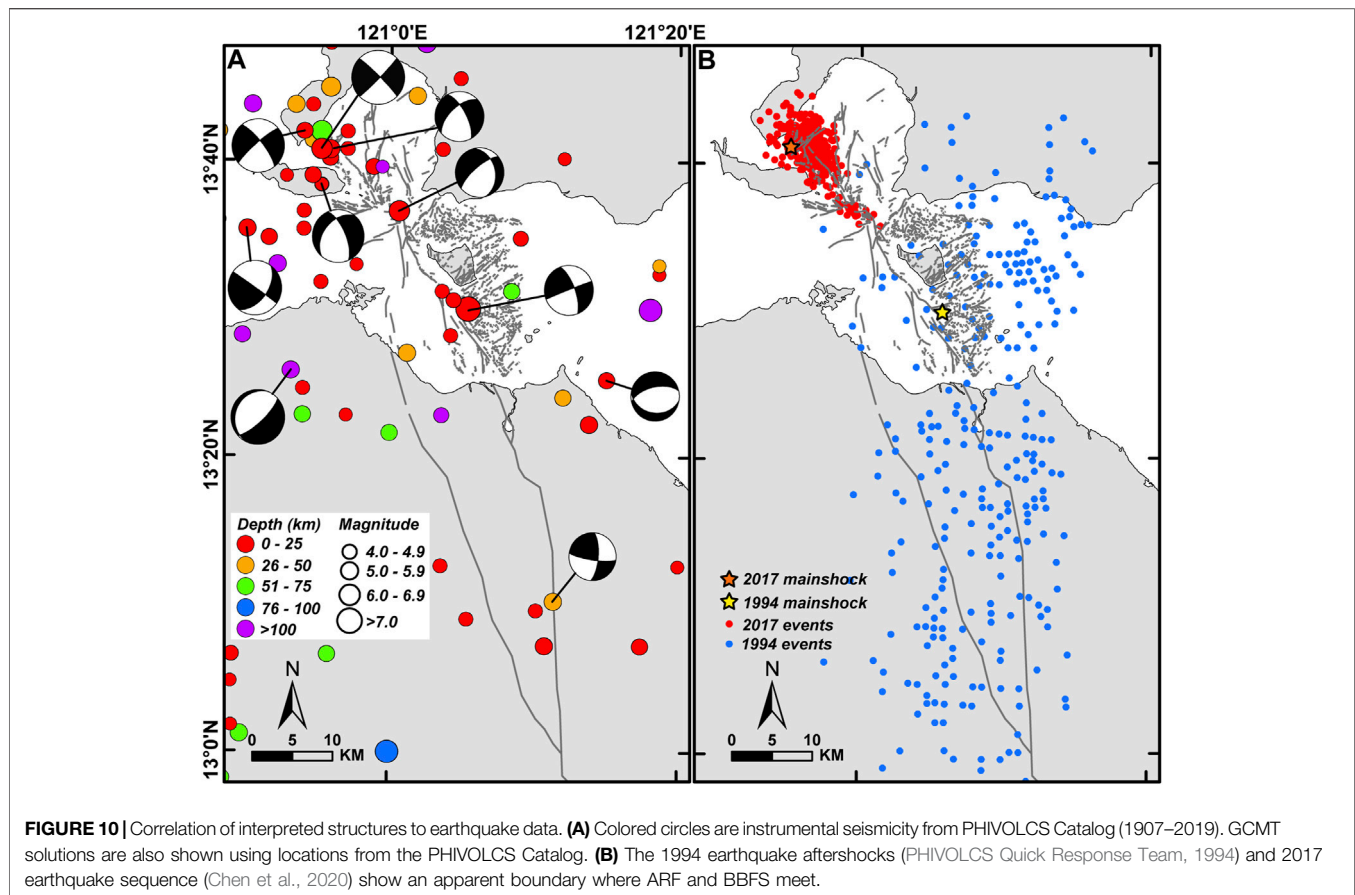
For the 2017 Mw 5.9 rupture on the Batangas Bay Fault System, stress change modelled was only up to ~ 0.5 bars (**Figure 11B**). Aglubang River Fault had positive change (<0.27 bars), increasing from south to north, except for an area nearest to the source fault which had a negative change of -0.47 bars. The two nearest receiver faults to the source showed stress increase: Batangas Bay Fault System at <0.30 bars and northern Central Mindoro Fault at <0.26 bars. Southern Central Mindoro Fault had negligible change (<0.009 bars). In the North Verde Fault System, the stress change in the normal faults ranged from -0.1 to 0.07 bars. The normal faults of the Central Verde Fault System had negative change (<-0.06 bars) while the left-lateral fault mostly gained stress (<0.07 bars). The stress change in the South Verde Fault ranges from -0.02 to -0.07 bars. The Northeast Mindoro Fault System gained stress (<0.08 bars). In general, the 2017 rupture caused a positive increase in the region fronting the southeastern end of the source fault with values decreasing with distance. The receiver fault planes far from the source fault (i.e., east of Aglubang River



Fault) experienced varying stress changes but within the same magnitude (mostly <0.1 bar change).

Coseismic coulomb stress changes for earthquake events from 1994 to 2017 were also correlated to the distribution of the relocated 2017 earthquake sequence (Chen et al., 2020). The first model (Figure 12A and Figure 12B) is a cumulative coseismic stress change after the 1994 earthquake and before the 2017 earthquake. Five earthquake events (1994–2001) were considered based on matching the GCMT events to the PHIVOLCS Catalog (1907–2019). The second model designated the 2017 mainshock as the source fault. Receiver faults for both models were set to match the fault plane of the 2017 mainshock. Results show that most of the 2017 earthquakes

plotted in the positive lobe of the cumulative 1994–2001 stress change (Figure 12A and Figure 12B). In particular, the Mw 5.9 mainshock and most events belonging to the 2017 foreshock sequence concentrated in the positive lobe of the cumulative stress change. Very few foreshock events plotted in the negative lobe. These events are notably very close to the time of the mainshock and therefore might be triggered by the earlier foreshock events. The aftershocks of the Mw 5.9 earthquake are mostly clustered along the fault plane (Figure 12C). Several events plotted in the positive lobe, implying triggering. However, there are also a significant number of aftershocks that plotted within the negative lobes of the 2017 earthquake, but still within the positive lobe of the cumulative 1994–2001 stress



change. Other factors might also influence the earthquake distribution, such as dynamic stress triggering, postseismic stress change, and interseismic loading. This could also be a product of the limitation of the designated source fault model and specified receiver fault.

DISCUSSION

A Conjugate Fault System in Offshore Southern Batangas and its Potential Seismic Hazard

Analysis of seafloor morphology revealed seven fault systems in Verde Island Passage and Batangas Bay (**Figure 9**). The F1 faults (Batangas Bay Fault System, Central Mindoro Fault, and Aglubang River Fault) define a long northwest-trending zone of semi-continuous right-lateral faults in the western part of the study region. In contrast, the F2 faults (Macolod Corridor, North Verde Fault System, Central Verde Fault System, and Northeast Mindoro Fault System) mainly consist of northeast-trending parallel left-lateral and normal faults approaching the northwest-trending zone of the F1 faults. The left-lateral South Verde Fault trends east-west and accommodates the motion between the Central Verde Fault System and the Northeast Mindoro Fault System. Overall, the patterns define conjugate

fault systems forming under approximately EW-directed extension.

GCMT focal mechanism solutions also indicate EW extension (Chen et al., 2020). The events from the 1994 and 2017 earthquakes plot near the traces of the Aglubang River Fault and the Batangas Bay Fault System (**Figure 10A**). Accurate determination of the fault rupture was not possible because of data limitations but is inferred on the fault trace nearest to the mainshock and consistent with the focal mechanism solution. The earthquake distribution from the two events (**Figure 10B**) shows an apparent boundary in the bathymetric relief in northern West Verde Basin (**Figure 2**; **Figure 3B**) where the trend of the right-lateral faults changes in a restraining manner. This restraining bend might have acted as a rupture barrier for both earthquakes. Furthermore, the northwestern distribution of the 2017 aftershocks was limited by the Calumpan Peninsula. This area consists of volcanic centers belonging to the Macolod Corridor and has a geothermal resource controlled by faults of varying trends (Del Rosario and Oanes, 2010). Both the high geothermal gradient and the structures might have stopped the further propagation of the aftershocks to the northwest (Chen et al., 2020).

The apparent connectivity of the Aglubang River Fault and the Batangas Bay Fault System implies possible contribution of the 1994 event to the occurrence of the 2017 event. Coulomb stress transfer model revealed that the Batangas Bay Fault System was

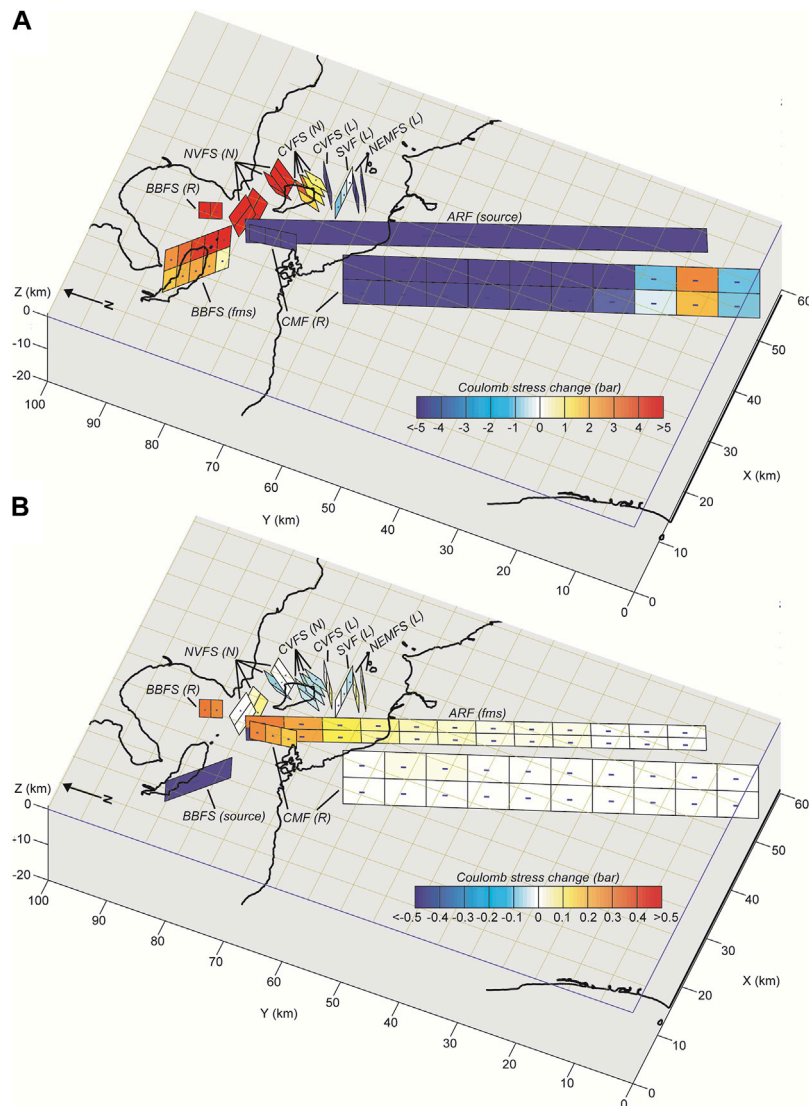


FIGURE 11 | Calculated Coulomb stress changes at $\mu' = 0.4$ on receiver faults in offshore southern Batangas during the **(A)** 1994 Mw 7.1 earthquake and **(B)** 2017 Mw 5.9 earthquake. Hotter colors indicate stress increase. ARF, Aglubang River Fault; CMF, Central Mindoro Fault; NVFS, North Verde Fault System; CVFS, Central Verde Fault System; SVF, South Verde Fault; NEMFS, Northeast Mindoro Fault System; BBFS, Batangas Bay Fault System. The letters in parenthesis indicate the fault geometry. R, pure right-lateral fault (dip/rake: $90^\circ/180^\circ$); L, pure left-lateral fault (dip/rake: $90^\circ/0^\circ$); N: pure normal fault (dip/rake: $60^\circ-90^\circ$); fms: derived from GCMT focal mechanism solution (ARF strike/dip/rake: $339^\circ/70^\circ/-178^\circ$; BBFS strike/dip/rake: $314^\circ/85^\circ/176^\circ$). The shorter fault models have downdip widths of 5 km while the longer faults have downdip widths of 15 km. Fault planes are divided based on their length and width to observe variations in stress received. Fault parameters are found in the Supplementary Material.

indeed brought closer to failure by 0.5–7.4 bars (**Figure 11**). Very few significant earthquakes occurred post-1994 and pre-2017 that might have influenced the occurrence of the 2017 earthquake sequence. Of the five significant earthquakes, the nearest to Batangas Bay is the 1997 Mw 5.4 event which occurred near the restraining bend of the F1 faults (**Figure 12A**). Cumulative stress change of the 1994 to pre-2017 earthquakes revealed that most events of the 2017 earthquake sequence plot within the positive lobe (**Figure 12A** and **Figure 12B**).

The question now is whether the other identified faults would also rupture in the future. Fault ruptures and stress triggering

along conjugate faults are not rare and some of the most recent earthquakes are of this type, such as the 2019 Ridgecrest Earthquake Sequence (e.g., Li S et al., 2020) and the 2019 Mindanao (Cotabato) Earthquake Sequence (e.g., Li B et al., 2020). The coseismic stress transfer models show that some of the fault planes surrounding the 1994 and 2017 rupture areas have experienced stress increase. While triggering may require a minimum stress change value, the value of this threshold widely varies (Steacy et al., 2005). However, it has been previously shown that an increase of 0.1 bar can change the rate of seismicity, ergo, increase in earthquake probability. The

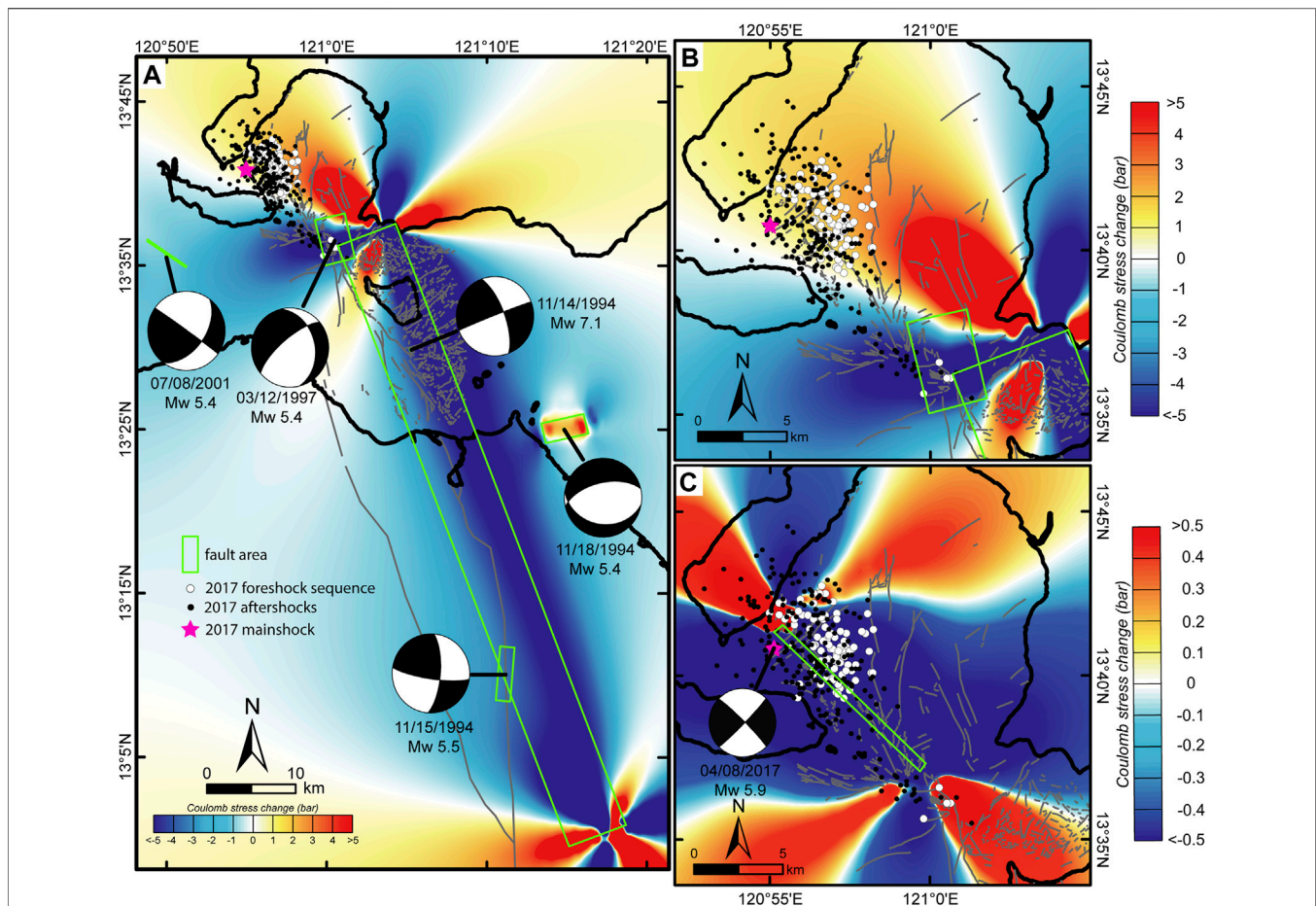


FIGURE 12 | Calculated Coulomb stress change at depth of 14.3 km with **(A and B)** cumulative 1994 to pre-2017 earthquakes and **(B)** 2017 Mw 5.9 Batangas Bay Fault System earthquake as source fault. The receiver fault for both calculations is specified as the same as the 2017 mainshock (strike/dip/rake: $314^{\circ}/85^{\circ}/176^{\circ}$) at $\mu' = 0.4$. The dots represent the relocated events from the 2017 earthquake sequence (Chen et al., 2020). White dots are the foreshock sequence while the black dots are the aftershocks. Dark gray lines are the interpreted faults. Green rectangles depict the source fault area. A purple star indicates the 2017 mainshock location.

1994 event caused a stress increase of >0.5 bars to most fault planes located near the northern end of the Aglubang River Fault and a portion of the Central Mindoro Fault to the south. On the other hand, the 2017 event increased the stress of several fault planes fronting the southeastern end of the source fault by up to 0.3 bars. Overall, the fault planes of Batangas Bay Fault System, North Verde Fault System, Central Verde Fault System, and Central Mindoro Fault gained significant stress. In terms of earthquake probability, stress change is interpreted to alter the time of the next earthquake (Stein, 1999; Toda and Stein, 2002). That is, an increase in stress would hasten the occurrence of the next earthquake while a decrease in stress would delay the occurrence. It is also important to acknowledge that other factors, such as dynamic stress, long-term loading, and other natural and human processes, can also affect the promotion of earthquake failures (Harris, 1998; Steacy et al., 2005).

It is therefore important to resolve how active are the identified faults and determine their recurrence intervals. This is to properly assess the timing of the next rupture and the effect of Coulomb stress transfer in altering the earthquake

probability. Unfortunately, this is one of the major limitations of this study. The faults in this work were only identified through its geomorphology. Aglubang River Fault is active and already ruptured in 1994. Onshore Central Mindoro Fault is designated active; however, the immediate offshore continuation coincides with an arcuate insular slope with no clear activity. The northernmost trace of the Central Mindoro Fault appears to be active which creates a scarp in the basin. Southwest Batangas Bay Fault System is associated with the 2017 rupture while the northeast Batangas Bay Fault System could be active, as evidenced by displaced gullies and offset reflectors. The NE-trending fault systems cut through crust belonging to the Mindoro Arc which has age dates from 0.82 to 1.64 Mya (de Boer et al., 1980), although the sample was from the volcanoes in northeast Mindoro coast. The Central Verde Fault System cuts through submarine terraces which makes it most likely to be active. Further studies must be done to constrain the seismogenic potential of these fault systems. Probable magnitudes were initially estimated from the longest surface fault trace from each fault system (**Table 1**) using fault-scaling

TABLE 1 | Probable magnitude from each fault system estimated from longest surface trace observed using fault-scaling relationship (Wells and Coppersmith, 1994).

Fault system	Longest fault segment observed (km)	Estimated moment magnitude
Batangas Bay Fault System	4.7	5.9
North Verde Fault System	5	5.8
Central Verde Fault System	9.1	6.2
South Verde Fault	6.1	6.0
NE Mindoro Fault System	4.7	5.9
Offshore Central Mindoro Fault	6.6	6.1
Onshore Central Mindoro Fault	113.6	7.5

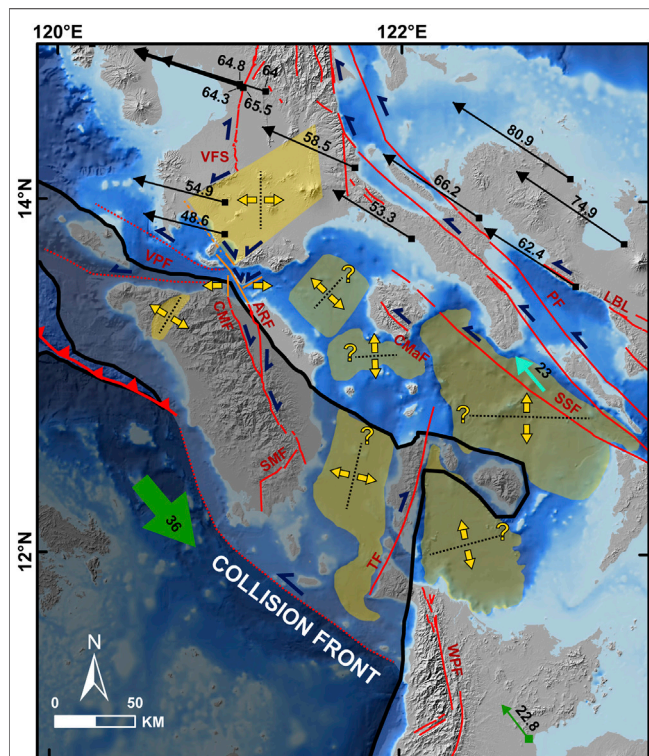


FIGURE 13 | Ongoing extension in northern Central Philippines because of differential northwestward block motion. Basins are delineated in yellow. The direction of extension for the basins are from the structural interpretation in Macolod Corridor (Pubellier et al., 2000) and T axes from GCMT solutions in other areas (Chen et al., 2015; Yoshida et al., 2016; Chen et al., 2020). Black arrows show GPS motions from Yu et al. (2013) while green arrows are from Rangin et al. (1999), all fixed to Sundaland Block in mm/yr. A light blue arrow indicates GPS-derived slip (mm/yr) of Sibuyan Sea Fault (SSF) fixed to Masbate Island (Bacolcol et al., 2005). Faults are from PHIVOLCS (2019), and the blue half arrows show direction of fault motion. The black line is the boundary of the Palawan Microcontinental Block (PCB) and the Philippine Mobile Belt (PMB). The PCB in a darker shade is the relatively less deformed North Palawan Block which is currently colliding with PMB. On the other hand, the PCB in a lighter shade is already emplaced in PMB and undergoing PMB-related deformation. VFS, Valley Fault System; VPF, Verde Passage Fault; ARF, Aglubang River Fault; CMF, Central Mindoro Fault; SMF, Southern Mindoro Fault; TF, Tablas Fault; WPF, West Panay Fault; CMaF, Central Marinduque Fault; SSF, Sibuyan Sea Fault; PF, Philippine Fault; LBL, Lake Bato Lineament.

relationships (Wells and Coppersmith, 1994). Several of these faults could still extend to the east, putting these estimates to a minimum.

Implications to Local and Regional Tectonics

The newly documented fault systems redefine the previously known faults in the region. The Verde Passage Fault does not run through the whole Verde Island Passage. Instead, a conjugate fault system characterizes the region around Verde Island. The South Verde Fault corresponds to the previous Verde Passage Fault trace south of Verde Island. Further investigations are needed to properly define the two branches of the Verde Passage Fault to the west which has clear bathymetric expression from the GEBCO bathymetric grid. On the other hand, Macolod Corridor appears to loosely terminate at Batangas Bay instead of the Verde Island Passage.

Despite being newly mapped tectonic features, the structures are still consistent with the known tectonics of the region (Figure 13). Focal mechanism solutions and conjugate fault patterns point to an approximately east-west extension (Chen et al., 2020). This is similar to the extension observed in the structural features in the Macolod Corridor (Pubellier et al., 2000). As such, the formation mechanism of the two regions must also be the same. Previous tectonic models indicate that the extension in southern Luzon accommodates the differential northwestward motion of several tectonic blocks. Velocity generally decreases from east of the Philippine Fault toward the Central Philippines where the Palawan Microcontinental Block-Philippine Mobile Belt collision impedes motion. The conjugate fault system in offshore Batangas is another addition to the extensional zones present in northern central Philippines which accommodate the necessary extension in between the collision zone and the Philippine Fault. However, it is noted here that while the extension direction in southern Luzon is east-west, the same direction is not consistent throughout northern central Philippines, as can be observed from the T axes from GCMT solutions (Yoshida et al., 2016) in Central Philippines (Figure 13).

This extension represents the most recent tectonic event in the Philippine Mobile Belt. Pubellier et al. (1997) referred to this as

the “post-docking” phase after the Palawan Microcontinental Block-Philippine Mobile Belt collision during the Middle Miocene (northern Philippines) to Pliocene (southern Philippines). The mapped conjugate faults straddle the Palawan Microcontinental Block-Philippine Mobile Belt boundary and affect both terranes. Some of the faults, like the F1 faults and the Verde Passage Fault, might have exploited and reactivated pre- and syn-collision structures. The Macolod Corridor and the other F2 faults cut through the NW-trending Southern Luzon Arc (with Mindoro Arc presumably inactive). Aglubang River Fault and Central Mindoro Fault, as well as South Mindoro Fault, displace the portion of the Palawan Microcontinental Block in Mindoro Island. Incidentally, other active structures that are not compressional (e.g., Wawa-Mamburao Valley extension, right-lateral Tablas Fault, other extensional basins in central Philippines) are also located within the Palawan Microcontinental Block near the collision zone. This means that the portion of the Palawan Microcontinental Block fronting the Philippine Mobile Belt, or the “emplaced” blocks, is also affected by the northwestward translation, as was noted by Pubellier et al. (1997). This implies that as the collision front migrated to its present position (i.e., south of Mindoro Island and west of Panay Island), the concurrently accreted crustal materials are subsequently affected by the existing stress regime within the Philippine Mobile Belt. Although the blocks belong to Palawan Microcontinental Block stratigraphically, the tectonic behavior of the emplaced blocks implies assimilation into the Philippine Mobile Belt.

Influence on Seafloor Morphology

The structures heavily influence the seafloor morphology in varying spatial scales. Localized extensions created basins and troughs while scarps and restraining beds are generated by uplift. Volcanic centers and aprons are displaced by normal faults. Linear ridges follow the general orientation of faults. Faults and lineaments dissect the shelves and slopes, and these are exploited by channels and gullies. Bottom current processes are evident in the basin floor (i.e., wide sediment wave fields, contourites). In the West Verde Basin, the sediment waves are in the uplifted parts of the seafloor. This suggests that the bottom current might experience velocity change as it encounters a significant bathymetric relief, thereby controlling the development of the sediment waves. Although in a deep-water fan environment, Maselli et al. (2021) demonstrated that active normal faulting triggered a hydraulic jump in the downslope evolution of turbidity currents, generating a stark contrast between the cyclic steps and antidunes in the footwall, and a featureless hanging wall. The bottom currents in the study region might experience a similar mechanism, and modeling must be done to prove this hypothesis. Meanwhile, the insular slopes have numerous landslide scarps. The oversteepening from long-term uplift creates unstable slopes which could collapse from gravity and/or additional triggering from coseismic ground motion from surrounding faults. For the 1994 Mindoro tsunamigenic earthquake, tsunami modeling suggested a submarine landslide source to augment the tsunami waves created by horizontal displacement (Tanioka

and Satake, 1996). Several landslide scarps are found along the Aglubang River Fault and around the West Verde Basin (Figure 2B), and therefore could be candidate sources for the 1994 tsunami.

CONCLUSION

High resolution marine geophysical data allowed characterization of seven fault systems defining a conjugate fault pattern in offshore southern Batangas. The conjugate fault system is compatible with the east-west extension in southern Luzon. Fault patterns, earthquake distribution, and Coulomb stress transfer modeling point to the promotion of failure of the 2017 earthquake along the Batangas Bay Fault System by the 1994 earthquake along the Aglubang River Fault. The stress transfer models indicate that the F1 faults (Batangas Bay Fault System and Central Mindoro Fault) and the northern F2 faults (North Verde Fault System and Central Verde Fault System) experienced stress increase. The identified faults, therefore, pose seismic hazards and more studies are needed to properly constrain their seismogenic potential and their possible extension to the surrounding unmapped region. Furthermore, the extensive slump scars indicate unstable insular slopes, therefore presenting future hazards and they must also be studied for their tsunamigenic potential.

DATA AVAILABILITY STATEMENT

The data analyzed in this study is subject to the following licenses/restrictions: Some of the datasets used in this study are courtesy of institutions (e.g., NAMRIA for multibeam bathymetry, PHIVOLCS for earthquake catalog, UP MSI for subbottom data) and are bound by agreements. Requests to access these datasets should be directed to NAMRIA (<https://www.namria.gov.ph/>), PHIVOLCS (<https://www.phivolcs.dost.gov.ph/>), and UP MSI (Dr. Fernando Siringan - fpsiringan@up.edu.ph).

AUTHOR CONTRIBUTIONS

KS conceptualized the study, conducted the data analysis, and wrote the paper. MA and FS provided supervision. KS, PF, and AC were involved in the subbottom data acquisition. FS secured the funding for this work. MA, PF, AC, BM, MA, AD, and FS provided critical feedback to the paper.

FUNDING

This research was supported by the joint research project of University of the Philippines-Marine Science Institute and the Department of Science and Technology - Philippine Institute of Volcanology and Seismology entitled “*Mapping of Active Offshore Faults for Resilient Coasts*” with funding from the Department of Science and Technology-Philippine Council for Industry, Energy,

and Emerging Technology Research and Development (DOST-PCIEERD) of the Republic of the Philippines. Additional funding was provided by the UP Marine Science Institute for the Verde Island Passage Cruise.

ACKNOWLEDGMENTS

The authors would like to thank the National Mapping and Resource Information Authority (NAMRIA) for generously providing the multibeam bathymetry data and the Department of Science and Technology - Philippine Institute of Volcanology and Seismology for providing the earthquake catalog. The research party and the ship crew of M/Y Panata of the University of the Philippines Marine Science Institute is also thanked for their assistance in data collection during the research

REFERENCES

- Aurelio, M. A., Barrier, E., Rangin, C., and Müller, C. (1991). The Philippine Fault in the Late Cenozoic Evolution of the Bondoc-Masbate-N. Leyte Area, Central Philippines. *J. South. Asian Earth Sci.* 6 (3-4), 221–238. doi:10.1016/0743-9547(91)90069-A
- Aurelio, M. A., Dianala, J. D. B., Taguibao, K. J. L., Pastoriza, L. R., Reyes, K., Sarande, R., et al. (2017). Seismotectonics of the 6 February 2012 Mw 6.7 Negros Earthquake, central Philippines. *J. Asian Earth Sci.* 142, 93–108. doi:10.1016/j.jseas.2016.12.018
- Aurelio, M. A., Peña, R. E., and Taguibao, K. J. L. (2013). Sculpting the Philippine Archipelago since the Cretaceous through Rifting, Oceanic Spreading, Subduction, Obduction, Collision and Strike-Slip Faulting: Contribution to IGMA5000. *J. Asian Earth Sci.* 72, 102–107. doi:10.1016/j.jseas.2012.10.007
- Aurelio, M. A. (2000). Shear Partitioning in the Philippines: Constraints from Philippine Fault and Global Positioning System Data. *Isl. Arc* 9 (4), 584–597. doi:10.1111/j.1440-1738.2000.00304.x
- Bacolcol, T., Barrier, E., Duquesnoy, T., Aguilar, A., Jorgio, R., de la Cruz, R., et al. (2005). GPS Constraint on Philippine Fault Slip Rate in Masbate Island, Central Philippines. *J. Geol. Soc. Philippines* 60 (1&2), 1–7.
- Barrier, E., Huchon, P., and Aurelio, M. (1991). Philippine Fault: A Key for Philippine Kinematics. *Geol* 19 (1), 32–35. doi:10.1130/0091-7613(1991)019<0032:pfpkfp>2.3.co;2
- Chen, P.-F., Olaver, E. A., Wang, C.-W., Bautista, B. C., Solidum, R. U., and Liang, W.-T. (2015). Seismotectonics of Mindoro, Philippines. *Tectonophysics* 640–641, 70–79. doi:10.1016/j.tecto.2014.11.023
- Chen, P.-F., Su, P.-L., Olaver, E. A., Jr., R. U. S., Jr., and Huang, B.-S. (2020). Relocation of the April 2017 Batangas, Philippines, Earthquake Sequence, with Tectonic Implications. *Terr. Atmos. Ocean. Sci.* 31, 273–282. doi:10.3319/TAO.2020.01.31.01
- de Boer, J., Odom, L. A., Ragland, P. C., Snider, F. G., and Tilford, N. R. (1980). The Bataan Orogen: Eastward Subduction, Tectonic Rotations and Volcanism in Western Pacific (Philippines). *Tectonophysics* 67 (3-4), 251–282. doi:10.1016/0040-1951(80)90270-X
- Defant, M. J., De Boer, J. Z., and Oles, D. (1988). The Western Central Luzon Arc, Two Arcs Divided by Rifting? *Tectonophysics* 145 (3-4), 305–317. doi:10.1016/0040-1951(88)90202-8
- Defant, M. J., Maury, R. C., Ripley, E. M., Feigenson, M. D., and Jacques, D. (1991). An Example of Island-Arc Petrogenesis: Geochemistry and Petrology of the Southern Luzon Arc, Philippines. *J. Petrol.* 32 (3), 455–500. doi:10.1093/ptrology/32.3.455
- Del Rosario, R. A., and Oanes, A. F. (2010). “Controlled Source Magnetotelluric Survey of Mabini Geothermal Prospect, Mabini, Batangas, Philippines,” in Proceedings of the World Geothermal Congress 2010, Bali, Indonesia, April 25–29, 2010.
- cruise in Verde Island Passage last July 2019. The authors are very much grateful to editor GR and reviewers YL and WF for providing valuable comments that greatly improved this manuscript. Topography data is from JAXA ALOS World 3D–30 m (AW3D30) DEM (<https://www.eorc.jaxa.jp/ALOS/en/aw3d30/index.htm>) while global bathymetry is from the GEBCO_2020 grid (https://www.gebco.net/data_and_products/gridded_bathymetry_data/). Focal mechanism solutions were obtained from Harvard GCMT (<https://www.globalcmt.org/>).

SUPPLEMENTARY MATERIAL

The Supplementary Material for this article can be found online at: <https://www.frontiersin.org/articles/10.3389/feart.2021.801670/full#supplementary-material>

- DeMets, C., Gordon, R. G., and Argus, D. F. (2010). Geologically Current Plate Motions. *Geophys. J. Int.* 181 (1), 1–80. doi:10.1111/j.1365-246X.2009.04491.x
- Dziewonski, A. M., Chou, T.-A., and Woodhouse, J. H. (1981). Determination of Earthquake Source Parameters from Waveform Data for Studies of Global and Regional Seismicity. *J. Geophys. Res.* 86 (B4), 2825–2852. doi:10.1029/jb086ib04p02825
- Foerster, H., Oles, D., Knittel, U., Defant, M. J., and Torres, R. C. (1990). The Macolod Corridor: a Rift Crossing the Philippine Island Arc. *Tectonophysics* 183 (1-4), 265–271. doi:10.1016/0040-1951(90)90420-D
- Gervasio, F. C. (1967). Age and Nature of Orogenesis of the Philippines. *Tectonophysics* 4 (4-6), 379–402. doi:10.1016/0040-1951(67)90006-6
- Harris, R. A. (1998). Introduction to Special Section: Stress Triggers, Stress Shadows, and Implications for Seismic hazard. *J. Geophys. Res.* 103 (B10), 24347–24358. doi:10.1029/98JB01576
- Karig, D. E. (1983). Accreted Terranes in the Northern Part of the Philippine Archipelago. *Tectonics* 2 (2), 211–236. doi:10.1029/TC002i02p0211
- King, G. C. P., Stein, R. S., and Lin, J. (1994). Static Stress Changes and the Triggering of Earthquakes. *B. Seismol. Soc. Am.* 84 (3), 935–953. doi:10.1785/BSSA0840030935
- Kociánová, L., and Melichar, R. (2016). OATools: An ArcMap Add-In for the Orientation Analysis of Geological Structures. *Comput. Geosciences* 87, 67–75. doi:10.1016/j.cageo.2015.12.005
- Li, B., Li, Y., Jiang, W., Su, Z., and Shen, W. (2020). Conjugate Ruptures and Seismotectonic Implications of the 2019 Mindanao Earthquake Sequence Inferred from Sentinel-1 InSAR Data. *Int. J. Appl. Earth Observation Geoinformation* 90, 102127. doi:10.1016/j.jag.2020.102127
- Li, S., Chen, G., Tao, T., He, P., Ding, K., Zou, R., et al. (2020). The 2019 Mw 6.4 and Mw 7.1 Ridgecrest Earthquake Sequence in Eastern California: Rupture on a Conjugate Fault Structure Revealed by GPS and InSAR Measurements. *Geophys. J. Int.* 221 (3), 1651–1666. doi:10.1093/gji/ggaa099
- Li, Y., Shao, Z., Shi, F., and Chen, L. (2020). Stress Evolution on Active Faults in the Southwestern Yunnan Region, southeastern Tibetan Plateau, and Implications for Seismic hazard. *J. Asian Earth Sci.* 200, 104470. doi:10.1016/j.jseas.2020.104470
- Marchadier, Y., and Rangin, C. (1990). Polyphase Tectonics at the Southern Tip of the Manila Trench: Mindoro-Tablas Islands, Philippines. *Tectonophysics* 183 (1-4), 273–287. doi:10.1016/0040-1951(90)90421-4
- Maselli, V., Micallef, A., Normandeu, A., Oppo, D., Iacopini, D., Green, A., et al. (2021). Active Faulting Controls Bedform Development on a Deep-Water Fan. *Geology* 49, 1495–1500. doi:10.1130/G49206.1
- Mines and Geosciences Bureau (2010). *Geology of the Philippines*. 2nd edition. Quezon City: Mines and Geosciences Bureau.
- Okada, Y. (1992). Internal Deformation Due to Shear and Tensile Faults in a Half-Space. *B. Seismol. Soc. Am.* 82 (2), 1018–1040. doi:10.1785/BSSA0820021018
- PHIVOLCS (2019). *Distribution of Active Faults and Trenches*. Quezon City: Philippine Institute of Volcanology and Seismology.

- PHIVOLCS Quick Response Team (1994). *15 November 1994 mindoro Earthquake: Preliminary Report of Investigation*. Quezon City: Philippine Institute of Volcanology and Seismology.
- Pinet, N., and Stephan, J. F. (1990). The Philippine Wrench Fault System in the Ilocos Foothills, Northwestern Luzon, Philippines. *Tectonophysics* 183 (1-4), 207–224. doi:10.1016/0040-1951(90)90417-7
- Pubellier, M., Aurelio, M., and Sautter, B. (2018). The Life of a Marginal basin Depicted in a Structural Map of the South China Sea. *Episodes* 41 (3), 139–142. doi:10.18814/epiugs/2018/018014
- Pubellier, M., Garcia, F., Loevenbruck, A., and Chorowicz, J. (2000). Recent Deformation at the junction between the North Luzon Block and the Central Philippines from ERS-1 Images. *Isl. Arc* 9 (4), 598–610. doi:10.1046/j.1440-1738.2000.00305.x
- Pubellier, M., Quebral, R., Aurelio, M., and Rangin, C. (1997). “Docking and Post-docking Escape Tectonics in the Southern Philippines”. In *Tectonic Evolution of Southeast Asia*. Editors R. Hall and D. Blundell (London: Geological Society of London), 511–523.
- Pubellier, M., Quebral, R., Rangin, C., Deffontaines, B., Muller, C., Butterlin, J., et al. (1991). The Mindanao Collision Zone: a Soft Collision Event within a Continuous Neogene Strike-Slip Setting. *J. Southe. Asian Earth* 6 (3-4), 239–248. doi:10.1016/0743-9547(91)90070-E
- Quebral, R. D., Pubellier, M., and Rangin, C. (1996). The Onset of Movement on the Philippine Fault in Eastern Mindanao: A Transition from a Collision to a Strike-Slip Environment. *Tectonics* 15 (4), 713–726. doi:10.1029/95TC00480
- Rangin, C., Le Pichon, X., Mazzotti, S., Pubellier, M., Chamot-Rooke, N., Aurelio, M., et al. (1999). Plate Convergence Measured by GPS across the Sundaland/Philippine Sea Plate Deformed Boundary: the Philippines and Eastern Indonesia. *Geophys. J. Int.* 139 (2), 296–316. doi:10.1046/j.1365-246x.1999.00969.x
- Rangin, C., Stephan, J. F., and Müller, C. (1985). Middle Oligocene Oceanic Crust of South China Sea Jammed into Mindoro Collision Zone (Philippines). *Geol* 13 (6), 425–428. doi:10.1130/0091-7613(1985)13<425:moocos>2.0.co;2
- Rangin, C. (1991). The Philippine Mobile Belt: a Complex Plate Boundary. *J. Southe. Asian Earth* 6 (3-4), 209–220. doi:10.1016/0743-9547(91)90068-9
- Rimando, J. M., Aurelio, M. A., Dianala, J. D. B., Taguibao, K. J. L., Agustin, K. M. C., Berador, A. E. G., et al. (2019). Coseismic Ground Rupture of the 15 October 2013 Magnitude (M W) 7.2 Bohol Earthquake, Bohol Island, Central Philippines. *Tectonics* 38 (8), 2558–2580. doi:10.1029/2019TC005503
- Rimando, R. E., Rimando, J. M., and Lim, R. B. (2020). Complex Shear Partitioning Involving the 6 February 2012 MW 6.7 Negros Earthquake Ground Rupture in Central Philippines. *Geosciences* 1011, 460. doi:10.3390/geosciences10110460
- Ringenbach, J. C., Stephan, J. F., Maletterre, P., and Bellon, H. (1990). Structure and Geological History of the Lepanto-Cervantes Releasing bend in the Abra River Fault, Luzon Central Cordillera, Philippines. *Tectonophysics* 183 (1-4), 225–241. doi:10.1016/0040-1951(90)90418-8
- Sarewitz, D. R., and Lewis, S. D. (1991). The Marinduque Intra-arc basin, Philippines: Basin Genesis and *In Situ* Ophiolite Development in a Strike-Slip Setting. *Geol. Soc. Am. Bull.* 103 (5), 597–614. doi:10.1130/0016-7606(1991)103<0597:tmiabp>2.3.co;2
- Sequeiros, O. E., Bolla Pittaluga, M., Frascati, A., Pirmez, C., Masson, D. G., Weaver, P., et al. (2019). How Typhoons Trigger Turbidity Currents in Submarine Canyons. *Sci. Rep.* 9, 9220. doi:10.1038/s41598-019-45615-z
- Stacy, S., Gombert, J., and Cocco, M. (2005). Introduction to Special Section: Stress Transfer, Earthquake Triggering, and Time-dependent Seismic hazard. *J. Geophys. Res.* 110, B05S01. doi:10.1029/2005JB003692
- Stein, R. S. (1999). The Role of Stress Transfer in Earthquake Occurrence. *Nature* 402, 605–609. doi:10.1038/45144
- Tanioka, Y., and Satake, K. (1996). Tsunami Generation by Horizontal Displacement of Ocean Bottom. *Geophys. Res. Lett.* 23 (8), 861–864. doi:10.1029/96GL00736
- Toda, S., and Stein, R. S. (2002). Response of the San Andreas Fault to the 1983 Coalinga-Nuñez Earthquakes: An Application of Interaction-Based Probabilities for Parkfield. *J. Geophys. Res.* 107 (B6), ESE 6-1–ESE 6-16. doi:10.1029/2001JB000172
- Toda, S., Stein, R. S., Sevilgen, V., and Lin, J. (2011). *Coulomb 3.3 Graphic-Rich Deformation and Stress-Change Software for Earthquake, Tectonic, and Volcano Research and Teaching—User Guide*. Virginia: U.S. Geological Survey.
- Toda, S., Stein, R. S., Reasenber, P. A., Dieterich, J. H., and Yoshida, A. (1998). Stress Transferred by the 1995Mw= 6.9 Kobe, Japan, Shock: Effect on Aftershocks and Future Earthquake Probabilities. *J. Geophys. Res.* 103 (B10), 24543–24565. doi:10.1029/98JB00765
- Tsutsumi, H., and Perez, J. S. (2013). Large-scale Active Fault Map of the Philippine Fault Based on Aerial Photograph Interpretation. *Acta Fault Res.* 39, 29–37. doi:10.11462/afr.2013.39_29
- Wang, R., Lorenzo-Martin, F., and Roth, F. (2006). PSGRN/PSCMP—a New Code for Calculating Co- and post-seismic Deformation, Geoid and Gravity Changes Based on the Viscoelastic-Gravitational Dislocation Theory. *Comput. Geosciences* 32, 527–541. doi:10.1016/j.cageo.2005.08.006
- Wells, D., and Coppersmith, K. (1994). New Empirical Relationships Among Magnitude, Rupture Length, Rupture Width, Rupture Area, and Surface Displacement. *Bull. Seismol. Soc. Am.* 84 (4), 974–1002. doi:10.1785/BSSA0840040974
- Yoshida, K., Pulido, N., and Fukuyama, E. (2016). Unusual Stress Rotations within the Philippines Possibly Caused by Slip Heterogeneity along the Philippine Fault. *J. Geophys. Res. Solid Earth* 121 (3), 2020–2036. doi:10.1002/2015JB012275
- Yu, S.-B., Hsu, Y.-J., Bacolcol, T., Yang, C.-C., Tsai, Y.-C., and Solidum, R. (2013). Present-day Crustal Deformation along the Philippine Fault in Luzon, Philippines. *J. Asian Earth Sci.* 65, 64–74. doi:10.1016/j.jseas.2010.12.007
- Yumul, G. P., Dimalanta, C. B., Marquez, E. J., and Queaño, K. L. (2009). Onland Signatures of the Palawan Microcontinental Block and Philippine mobile belt Collision and Crustal Growth Process: a Review. *J. Asian Earth Sci.* 34, 610–623. doi:10.1016/j.jseas.2008.10.002

Conflict of Interest: The authors declare that the research was conducted in the absence of any commercial or financial relationships that could be construed as a potential conflict of interest.

Publisher’s Note: All claims expressed in this article are solely those of the authors and do not necessarily represent those of their affiliated organizations, or those of the publisher, the editors, and the reviewers. Any product that may be evaluated in this article, or claim that may be made by its manufacturer, is not guaranteed or endorsed by the publisher.

Copyright © 2022 Sarmiento, Aurelio, Flores, Carrillo, Marfito, Abigania, Daag and Siringan. This is an open-access article distributed under the terms of the Creative Commons Attribution License (CC BY). The use, distribution or reproduction in other forums is permitted, provided the original author(s) and the copyright owner(s) are credited and that the original publication in this journal is cited, in accordance with accepted academic practice. No use, distribution or reproduction is permitted which does not comply with these terms.